

Special Observing Period (SOP) Data for the Year of Polar Prediction site Model Intercomparison Project (YOPPsiteMIP)

Zen Mariani¹, Sara M. Morris^{2,11}, Taneil Uttal², Elena Akish^{3,2}, Robert Crawford¹, Laura Huang¹, Jonathan Day⁴, Johanna Tjernström¹², Øystein Godøy¹², Lara Ferrighi¹², Leslie M. Hartten^{3,2}, Jareth Holt⁶, Christopher J. Cox², Ewan O'Connor⁹, Roberta Pirazzini⁹, Marion Maturilli¹³, Giri Prakash¹⁰, James Mather⁸, Kimberly Strong⁵, Pierre Fogal⁵, Vasily Kustov^{7,14}, Gunilla Svensson⁶, Michael Gallagher^{3,2}, Brian Vase¹¹

¹Meteorological Research Division, Environment and Climate Change Canada, Toronto, Canada

²NOAA Physical Sciences Laboratory, Boulder, CO, USA

³Cooperative Institute for Research in Environmental Science, University of Colorado, Boulder, Colorado, USA

⁴European Centre for Medium-Range Weather Forecasts, Reading, UK

⁵Department of Physics, University of Toronto, Toronto, Canada

⁶Department of Meteorology, Stockholm University, Sweden

⁷Arctic and Antarctic Research Institute, Air-sea interaction department, St. Petersburg, Russia

⁸Pacific Northwest National Laboratory, Richland, WA, USA

⁹Finnish Meteorological Institute, Finland

¹⁰Environmental Sciences Division, Oak Ridge National Laboratory, Oak Ridge, TN, USA

¹¹NOAA Global Monitoring Laboratory, Boulder, CO, USA

¹²Norwegian Meteorological Institute, Norway

¹³Alfred Wegener Institute, Helmholtz Centre for Polar and Marine Research, Potsdam, Germany

¹⁴Freelance entrepreneur, Belgrade, Serbia

Correspondence to: Zen Mariani (zen.mariani@ec.gc.ca) and Sara Morris (Sara.Morris@noaa.gov)

Abstract. The rapid changes occurring in the polar regions require an improved understanding of the processes that are driving ~~the~~these changes. At the same time, increased human activities, such as marine navigation, resource exploitation, aviation, commercial fishing, and tourism, require reliable and relevant ~~weather~~ information. One of the primary goals of the World Meteorological Organization's Year of Polar Prediction (YOPP) Project is to improve the accuracy of numerical weather prediction (NWP) at high latitudes. During YOPP, two Canadian ~~observatories~~supersites were commissioned and equipped with new ground-based instruments for enhanced meteorological and system process observations ~~that are considered to be "supersites" for addressing YOPP objectives, while other. Additional~~ pre-existing supersites in Canada, the United States, Norway, Finland, and Russia ~~also~~ provided data from ongoing long-term observing programs. ~~Data from these seven supersites were amalgamated and are being used to evaluate NWP systems from several international forecast centers and to perform meteorological process studies with the aim~~These supersites collected a ~~wealth of~~ improving NWP performance in the Polar Regions~~observations that are well-suited to address YOPP objectives.~~ In order to increase data useability and station interoperability, novel Merged Observatory Data Files (MODFs) ~~have been~~were created for ~~these~~the seven ~~international~~ supersites over two Special Observing Periods (February to March 2018 and July to September 2018).

39 All observations collected at the ~~seven~~ supersites were compiled into this ~~new~~ standardized NetCDF MODF format,
40 simplifying the process of conducting pan-Arctic NWP verification and process evaluation studies. This paper describes the
41 seven Arctic YOPP supersites, their instrumentation, data collection and processing methods, ~~and~~ the novel MODF format
42 and output files, which together, and examples of the observations contained therein. MODFs comprise the observational
43 contribution to the ~~associated~~ model intercomparison effort, termed YOPP supersite Model Intercomparison Project
44 (YOPPsiteMIP). All YOPPsiteMIP MODFs are publicly accessible via the YOPP Data Portal (Whitehorse:
45 <https://doi.org/10.21343/a33e-j150>, Iqaluit: <https://doi.org/10.21343/yrnf-ck57>, Sodankylä: [https://doi.org/10.21343/m16p-](https://doi.org/10.21343/m16p-pq17)
46 [pq17](https://doi.org/10.21343/a2dx-nq55), Utqiagvik: <https://doi.org/10.21343/a2dx-nq55>, Tiksi: <https://doi.org/10.21343/5bwn-w881>, Ny-Ålesund:
47 <https://doi.org/10.21343/y89m-6393>, Eureka: <https://doi.org/10.21343/r85j-tc61>), hosted by MET Norway, with
48 corresponding output from NWP models.

49 **1 Introduction**

50 In the Arctic there is a recognized lack of process-level information supplementing meteorological observations to characterize
51 the atmosphere and the cryosphere for operational forecasting (Cassano et al., 2011; Illingworth et al., 2015; Lawrence et al.,
52 2019). As the climate continues to change, information on weather and climate is becoming more critical in ensuring the health
53 and safety of local communities. Unfortunately, climate models do a poor job of capturing key features of Arctic climate, such
54 as the Arctic amplification factor, likely as a result of inaccurate representation of key physical processes, as shown by
55 Rantanen et al. (2022). Similarly, the accuracy of weather forecasts in the Polar Regions is also lower than in mid-latitudes
56 (Jung et al., 2016) partly due to the scattered and limited availability of observing networks (Lawrence et al., 2019). Advances
57 in Polar weather forecast prediction are expected to improve weather forecasts and climate predictions elsewhere (Jung et al.,
58 20142016 and Day et al., 2019), but understanding the causes of poor model performance in the Arctic is limited by the
59 availability of observatory data. Data from observatories, where sometimes hundreds of parameters are measured, are needed
60 for detailed investigations into the cause of model error, such as boundary-layer processes and turbulent exchanges (e.g., Day
61 et al., 20232024).

62
63 To address the need to improve Numerical Weather Prediction (NWP) performance in the Polar Regions, the World
64 Meteorological Organization (WMO) launched the international Polar Prediction Project with its flagship activity, the Year of
65 Polar Prediction (YOPP). During YOPP's core phase, from mid-2017 to mid-2019, several intensive observing periods were
66 conducted with close coordination between the international network of polar observatories and weather forecast centers. The
67 aim was to produce highly-concentrated sets of observed and modelled data for supporting forecast evaluation and process
68 studies (Koltzow et al., 2019; Goessling et al., 2016; Jung et al., 2016).

70 One of the flagship activities of YOPP was the YOPP supersite Model Intercomparison Project (YOPPsiteMIP), an initiative
71 to assess the performance of NWP systems at the process level by comparing with observatory data (Day et al., [20232024](#)).
72 To achieve this, a dataset of weather forecasts was produced by various NWP centers for supersite locations. In the Arctic
73 dataset covers two Special Observing Periods (SOPs), SOP1 (February 1 – March 31, 2018) and SOP2 (July 1 – September
74 30, 2018). During this period the number of routine observations (e.g. radiosonde launches, buoy deployments, etc.) were
75 enhanced in the Arctic (doubled in the case of radiosondes), field campaigns were conducted, and enhanced observations from
76 the designated YOPP “supersite” observatories were taken. [In general, the suite of several additional instruments that enable
77 an enhanced measurement program, including remote sensing, radiation, and other meteorological sensors, is what
78 distinguishes a ‘supersite’ from a typical weather site.](#) This paper documents the efforts to compile the supersite ([hereafter
79 referred to as “sites”](#)) data collected during this period as part of the YOPPsiteMIP. These [supersitesites](#) (Figure 1) are
80 distributed over a diverse range of geographical locations capturing some of the diversity in the terrestrial high-latitude climate
81 zones.

82
83 Prior to YOPP, data collection, processing, geophysical variable reporting cadences, and file output type and format were not
84 standardized across the [supersitesites](#), which are operated by different international agencies and consortiums. This lack of
85 interoperability made performing multi-site comparisons, evaluations, and process studies difficult and time consuming,
86 deterring potential users of [supersitethe](#) data (Wohner et al., 2022). In order to address this problem, the concept of standardized
87 Merged Observatory Data Files (MODFs) was developed as part of the YOPPsiteMIP (Uttal et al., [20232024](#)). This concept
88 is based on combining measurements from multiple international research observatories’ instruments into a single NetCDF
89 file that complies with established data management standards. Prior to MODFs, there generally existed no standardized
90 procedures for coordinated data management at these research sites such as those that have been developed for operational
91 datasets. Thus, the data from these sites’ separate instruments were scattered between separate files with different authors,
92 formats, metadata, post-processing techniques, physical archive locations, and requirements for usage. As such, they could not
93 be amalgamated to provide a pan-Arctic observational dataset.

94
95 MODF files bring together observations from different earth system components in a standardized NetCDF file format to
96 enable utilization of research-grade, process-level observations for model evaluation and parameterization development. At
97 the same time, MODFs are compatible with and mirror Merged Model Data Files (MMDFs) that are produced by each NWP
98 centre participating in YOPP (Day et al., [20232024](#)). Each geophysical variable observed at a site is matched to its
99 corresponding NWP model geophysical variable using [identical a standardized](#) data format, cadence, and file structure ~~in order
100 to facilitate improved observation model comparisons at the supersites (Gallagher and Tjernström, 2024).~~ Uttal et al.
101 ([20232024](#)) provides a generalized overview for the content and data structure of MODFs, i.e., a single NetCDF data file
102 containing measurements from multiple sources, and a series of tools to facilitate their creation. [Table 1 provides information](#)

103 regarding the on-site facility location where measurements were collected and their coordinates for reference. For some sites
104 (e.g., Sodankylä), certain geophysical variables are measured at multiple locations; these are all reported in the MODF with
105 their corresponding measurement coordinates embedded within the file so as to distinguish each measurement. Final DOIs for
106 the MODF_{yms} are listed in Table 2.

107
108 The MODF's standardized file structure directly aligns with the NWP's MMDFs. Thus, MODFs easily facilitate observation-
109 model comparisons at any/all of the seven sites (Gallagher and Tjernström, 2024). The purpose of the present work is to
110 describe the construction and contents of MODFs for seven of the YOPP-designated Arctic ~~supersites~~ sites during SOPs 1 and
111 2 (hereafter, "MODF_{ysm}"): Whitehorse, Canada (60.71 °N, 135.07 °W, 682 m a.s.l.); Iqaluit, Canada (63.74 °N, 68.51 °W, 11
112 m a.s.l.); Sodankylä, Finland (67.367 °N, 26.629 °E, 179 m a.s.l.); Utqiagvik (Barrow), Alaska (71.325 °N, 156.625 °W, 8 m
113 a.s.l.); Tiksi, Russia (71.596 °N, 128.889 °E, 30 m a.s.l.); Ny-Ålesund, Norway (78.923 °N, 11.926 °E, 15 m a.s.l.); and Eureka,
114 Canada (80.083 °N, 86.417 °W, 89 m a.s.l.). Methods used to organize a site's dataset and develop MODFs are provided. Each
115 sites' instrumentation and data processing are also described in this work to provide users with additional context and
116 information about the source of the geophysical variables contained in the MODF. The MODFs' counterpart, MMDFs, are
117 described in Uttal et al. (2024). ~~Table 1 provides information regarding the on-site facility location where measurements were~~
118 ~~collected and their coordinates for reference. For some sites (e.g., Sodankylä), certain geophysical variables are measured at~~
119 ~~multiple locations; these are all reported in the MODF with their corresponding measurement coordinates embedded within~~
120 ~~the file so as to distinguish each measurement. These MODFs closely mirror the format used to archive the YOPPsiteMIP~~
121 ~~NWP data, in order to enable model evaluation. Final DOIs for the MODF_{yms} are listed in Table 2.~~

122
123 Creating a standardized dataset such as MODF that contains observations from different meteorological and research agencies'
124 sites is an extremely complex, non-trivial task. For the sake of brevity and to reduce redundancy, this paper references site- or
125 instrument-specific publications in order to fully describe all of the aspects of the MODF dataset, including instrumentation,
126 quality control, (QC), and processing techniques. In the case where non-trivial aspects about the MODF data arise, the data's
127 origin, reference publications (e.g., dataset dois), and site contacts have been provided. Section 2 describes the data processing
128 chain conducted at each ~~supersite~~ site, including information about the site's local topography, climate, and instrumentation in
129 order to provide site-specific context to aid the interpretation of model-observation comparisons. Section 3 describes the
130 instrumentation and calculated variables. Section 4 describes the standardized MODF dataset file format, ~~quality control~~ QC,
131 and post processing, which in some cases differed slightly from site-to-site. Section 5 describes the MODF data structure,
132 attributes, and example Figures that illustrate the available dataset. Data and code availability is provided in Section 6, and
133 concluding remarks are provided in Section 7.

134 2 Site Descriptions

135 ~~It is important to~~To properly contextualize and interpret the observations contained within the MODF since they come from
136 vastly different sites. A map of the distribution of the ~~supersites is shown in Figure 1 and local maps showing the vicinity~~
137 ~~around each supersite are found in Figure 2. For context, also shown in Figure 2, are native spatial grids of the forecast models~~
138 ~~that participated in YOPPsiteMIP. While all supersites sites is shown in Figure 1. While all sites~~ are also designated surface
139 synoptic observation (SYNOP) stations, the meteorological data provided in the MODFs is significantly more detailed and
140 includes additional geophysical variables and thus is not the same as the SYNOP data. Table 3 lists the geophysical variables
141 observed at each site that are stored in the standardized MODF format, their measurement location(s), and other attributes; the
142 MODF featureType corresponds to the type of geophysical variable being observed at each site (they are split up into broad
143 categories). ~~Note that all radiation sensor footprints are ~0.2 m in diameter and have a dome of ~5 cm in diameter.~~

144 2.1 Whitehorse, Canada

145 The Whitehorse ~~supersitesite~~ (Figure 2) was commissioned as part of the Canadian Arctic Weather Science (CAWS) project
146 (Mariani et al., 2018; Joe et al., 2020). ~~CAWS was initiated to evaluate upper air observing technologies that can complement~~
147 ~~and improve Polar forecasts, perform satellite calibration / validation over Arctic terrain, and to provide recommendations to~~
148 ~~optimize the Canadian Arctic observing network. The supersite'ssite's~~ instruments (Figure 2 and Table 4) are installed on an
149 elevated platform, all within a few meters of each other. ~~Whitehorse has a population greater than 26,000 inhabitants. It is the~~
150 ~~primary gateway for air traffic for all of the Yukon Territories, parts of Alaska, and the Western Canadian Arctic. The~~
151 ~~supersiteThe site~~ is located at the Erik Nielsen Whitehorse International Airport, which is situated on a plateau ~50 m above
152 the rest of the city. The city is located in a valley between the Yukon Ranges to its West (~1.6 km a.s.l.) and East (~1.4 km
153 a.s.l.); this complex mountainous terrain strongly influences the weather systems that reach Whitehorse, which mostly originate
154 from the Eastern Pacific or over Alaska.

155
156 ~~Whitehorse experiences cold to temperate average monthly temperatures ranging from -15 to 14 °C (annual mean of -2 °C)~~
157 ~~and average monthly precipitation ranging from 7 to 38 mm (annual total of ~500 mm). Since the city is in the rain shadow of~~
158 ~~the Coast Mountains, precipitation totals are relatively low year-round. The primary surface wind direction follows the valley~~
159 ~~(NNW) and the average roughness length is estimated to be 1.0 m (Pinard et al., 2005). The soil type at and around the site is~~
160 a mixture of grained alluvial and colluvial slopes and, as part of the Boreal Cordillera ecozone, the surface type is primarily
161 Boreal Forest, including complex plateaus, mountains, valleys and Cordilleran vegetation. ~~Whitehorse experiences cold to~~
162 ~~temperate average monthly temperatures ranging from -15 to 14 °C and average monthly precipitation ranging from 7 to 38~~
163 ~~mm. Since the town is in the rain shadow of the Coast Mountains, precipitation totals are relatively low year-round. With a~~

164 population greater than 26,000 inhabitants. Whitehorse is the primary gateway for air traffic for all of the Yukon Territories,
165 parts of Alaska, and the Western Canadian Arctic. During the YOPP SOPs, radiosondes were launched four times daily.

166 2.2 Iqaluit, Canada

167 Like Whitehorse, the Iqaluit ~~supersitesite~~ (Figure 3) was commissioned as part of the CAWS project (Mariani et al., 2022).
168 ~~It~~The site is located ~200 m from the airport runway and all instruments (Figure 3 and Table 5) are co-located to within no
169 more than 140 m of each other on flat terrain. ~~Co-located instrument evaluation studies were conducted for several remote~~
170 ~~sensing and upper air observations (Mariani et al., 2020, 2021), including preliminary model verification studies during the~~
171 ~~YOPP SOPs and beyond. Iqaluit has over 8,000 inhabitants and is the primary gateway for air and sea traffic for the central~~
172 ~~and Eastern Canadian Arctic. The city itself is located along the coast in a valley that runs in the NW to SE direction; thus, the~~
173 primary direction of surface winds, which are frequently severe ($> 15 \text{ m/sms}^{-1}$), follows this direction. The surrounding region
174 is relatively flat Arctic tundra except for nearby hills (~300 m a.s.l.) approximately two kilometers to the NE of the ~~supersite~~.
175 ~~The average roughness length determined from the variance of wind speed is 0.14 m (Gordon et al., 2010)-site.~~

176
177 Iqaluit experiences an extreme range of average monthly temperatures ranging from -28 to 8 °C (annual mean of -9 °C) and
178 average monthly precipitation ranging from 18 to 70 mm (annual total of ~460 mm). The soil type at and around the site is
179 cryosolic and the surface type is ~70% tundra and ~30% ocean within a 10 km radius of the ~~supersitesite~~. Most storm tracks
180 that reach Iqaluit originate over the Western Canadian Arctic or the Prairies; these storms can produce strong Easterly winds
181 which frequently cause blowing snow that severely reduces visibility during non-summer months. Given the site's proximity
182 to Frobisher Bay (< 600 m), the site is influenced by sea surface conditions during onshore flow (NW). ~~Iqaluit experiences an~~
183 ~~extreme range of average monthly temperatures ranging from -28 to 8 °C and average monthly precipitation ranging from 18~~
184 ~~to 70 mm.~~

185 Co-located instrument evaluation studies were conducted for several remote sensing and upper air observations (Mariani et
186 al., 2020, 2021), including preliminary model verification studies during the YOPP SOPs and beyond. Iqaluit has over 8,000
187 inhabitants and is the primary gateway for air and sea traffic for the central and Eastern Canadian Arctic. During the YOPP
188 SOPs, radiosondes were launched four times daily.

189 2.3 Sodankylä, Finland

190 The Sodankylä ~~supersitesite~~ (Figure 4) is managed by the Arctic Space Centre of the Finnish Meteorological Institute (FMI-
191 ARC) ~~and~~. It is located in the Scandinavian taiga, which consists of a mix of spruces, pines and birches. The
192 ~~measurementsinstruments~~ (Figure 4 and Table 6) at the Sodankylä ~~supersitesite~~ are distributed over seven main observational

193 sites, each of them including several installations (48m, 24m, 20m or 16m towers, automatic weather stations (AWS),
194 structures supporting snow and soil measurements) that cover an area of approximately 1.5 km². The environment of the
195 observational sites varies between dense forest, sparse forest, forest openings, and wetland, each of these environments having
196 its own particular surface characteristics. ~~The supersite~~

197
198 ~~Sodankylä experiences monthly temperatures ranging from -11 to 15 °C (annual mean of 1 °C) and average monthly~~
199 ~~precipitation ranging from 35 to 85 mm (annual total of ~660 mm). The site~~ is a calibration/validation site for numerous
200 satellite products (such as snow water equivalent and snow extent (Luoju et al., 2021), and soil freeze-thaw (Cohen et al.,
201 2021 and Rautiainen et al., 2016), ~~hence the~~). ~~The~~ spatial distribution of the observational sites reflects the need of measuring
202 the spatial variability of observed parameters over different spatial scales and satellite footprints (Hannula et al., ~~2016~~-2016).
203 ~~During the YOPP SOPs, radiosondes were launched four times daily.~~

204 2.4 Utqiagvik (formerly Barrow), USA

205 The Utqiagvik ~~supersite~~ (Figure 5) consists of observatories located ~3 km southeast from the coastline where the Beaufort
206 and Chukchi Seas meet. The ~~supersite~~ is situated over tundra interspersed with thermokarst lakes having a coverage of up
207 to 40% area (Sellmann et al., 1975). ~~There are two primary observatories located outside of Utqiagvik (formerly Barrow),~~
208 ~~Alaska: The Atmospheric Radiation Measurement (ARM) North Slope of Alaska (NSA) observatory operated by the~~
209 ~~Department of Energy (DOE), and the Barrow Atmospheric Baseline Observatory facility operated by the National Oceanic~~
210 ~~and Atmospheric Administration (NOAA) Global Monitoring Laboratory (GML). These observatories are equipped with a~~
211 ~~suite of meteorological instruments (Figure 5 and Table 7) located 8 km east of the town of Utqiagvik. This is likely beyond~~
212 ~~the influence of a local heat island in town (Hinkel et al., 2007) and disturbance to snow cover by human activity (Stone et al.,~~
213 ~~2002). The site includes several towers and space for guest instruments.~~

214
215 ~~Utqiagvik experiences monthly temperatures ranging from -26 to 9 °C (annual mean of -10 °C) and average monthly~~
216 ~~precipitation ranging from 35 to 85 mm (annual total of ~770 mm). The climate in Utqiagvik, and much of the Alaskan North~~
217 Slope, is regulated by seasonal sea ice cover and the dominance of easterlies that circulate around the Beaufort High. This
218 atmospheric pattern is punctuated by episodes of southerly advection of air masses from the north Pacific, which frequently
219 arrive from the direction of the Bering Strait and are influential the timing of seasonal transitions of terrestrial snow cover and
220 sea ice coverage in both autumn and spring (Cox et al., 2017).

221
222 ~~There are two primary observatories located outside of Utqiagvik (formerly Barrow), Alaska: The Atmospheric Radiation~~
223 ~~Measurement (ARM) North Slope of Alaska (NSA) observatory operated by the Department of Energy, and the Barrow~~

224 Atmospheric Baseline Observatory facility operated by the NOAA Global Monitoring Laboratory (GML). These observatories
225 are located 8 km east of the town of Utqiagvik, and likely beyond the influence of a local heat island in town (Hinkel et al.,
226 2007) and disturbance to snow cover by human activity (Stone et al., 2002). The site includes several towers and space for
227 guest instruments. The GML Barrow Atmospheric Baseline Observatory recently built a newly furnished on-site laboratory
228 that was completed in 2020. The site's previous facility was constructed in 1972
229 (<https://gml.noaa.gov/obop/brw/history/index.html>), and was deconstructed in 2021. The ARM NSA observatory was
230 established in 1997 (Verlinde et al., 2016). Together, the GML and ARM observatories provide an extensive set of long-term
231 measurements at this coastal location. Measurements include properties of aerosols, clouds, precipitation, trace gases, the
232 atmospheric state and the surface energy balance. Radiosondes Unlike the other YOPP sites, radiosondes were launched three
233 times daily during the SOPs specifically in response to a WMO YOPP organizational request.

234 2.5 Tiksi, Russia

235 The Tiksi observatory (Figure 6) The original Tiksi science station was established in 1932 and at its height had 60-80 staff
236 and families that lived onsite with a school and grocery store comprising an independent community. The current Tiksi
237 observatory, in the same location, is 7 km away from the town of Tiksi, Russia, in the Sakha Republic of northern Siberia and
238 is staffed by personnel that commute from the town. Tiksi hosts a 20-m flux tower, a clean air facility, a weather station, a
239 Climate Reference Network (CRN) platform, and a Baseline Surface Radiation Network (BSRN) platform, among other
240 instruments (Figure 6 and Table 8) (Ohmura et al., 1998; Driemel et al., 2018). In collaboration with the Russian Federal
241 Service for Hydrometeorological and Environmental Monitoring (Roshydromet), a partnership was established with the
242 National Oceanic and Atmospheric Administration (NOAA) and the Finnish Meteorological Institute (FMI) in 2005 to collect
243 climate grade meteorological, surface energy budget, greenhouse gases and aerosol data (Uttal et al., 2013). The Tiksi station
244 is a coastal site, with facilities built in a high latitude tundra regime, comprising several different types of tundra land
245 classifications including shrub (most predominant), lichen, wet/dry fen, grassy, bog, water, bare and meadow (Mikola et al.,
246 2018).

247
248 On site, Tiksi hosts a 20-m flux tower, a clean air facility, a weather station, a Climate Reference Network (CRN) platform,
249 and a Baseline Surface Radiation Network (BSRN) platform (Ohmura et al., 1998; Driemel et al., 2018). Radiosonde data
250 were incorporated into the Integrated Global Radiosonde Archive (IGRA) and are available through NOAA's National Centers
251 for Environmental Information (NCEI) portal (Durre et al., 2018). Radiosondes had twice daily launches during the SOPs
252 specifically in response to a WMO YOPP organizational request. Meteorologically, Tiksi is located in a boundary region
253 between Atlantic and Pacific air masses. The resulting variability in atmospheric conditions with air masses originating from
254 various source regions in Russia, Northern America, Europe and Central Asia require careful attention and interpretation of

255 in-situ measurements. Tiksi is also influenced by its location at the mouth of the Lena River, the second largest river draining
256 into the Arctic Ocean and the only major Russian river underlain by permafrost which has impacts on the processes and
257 evolution of surface fluxes. Tiksi is also situated on the coast of the Laptev Sea, which is historically a region of large sea-ice
258 production.

259
260 Tiksi experiences monthly temperatures ranging from -29 to 11 °C (annual mean of -10 °C) and average monthly precipitation
261 ranging from 15 to 65 mm (annual total of ~510 mm). The original Tiksi science station was established in 1932 and at its
262 height had 60-80 staff and families that lived onsite with a school and grocery store comprising an independent community.
263 In collaboration with the Russian Federal Service for Hydrometeorological and Environmental Monitoring (Roshydromet), a
264 partnership was established with NOAA and the FMI in 2005 to collect climate grade meteorological, surface energy budget,
265 greenhouse gases and aerosol data (Uttal et al., 2013). Radiosonde data were incorporated into the Integrated Global
266 Radiosonde Archive (IGRA) and are available through NOAA's National Centers for Environmental Information (NCEI)
267 portal (Durre et al., 2018). Unlike the other YOPP sites, radiosondes had twice daily launches during the SOPs.

268 2.6 Ny-Ålesund, Norway

269 At Ny-Ålesund Research Station (Figure 7) in Svalbard, Norway, multi-disciplinary observations are operated by several
270 institutions of different nationalities. The Norwegian Meteorological Institute (aka MET Norway; www.met.no) is operating
271 the standard meteorological surface and synoptic observations (Figure 7 and Table 9) reported to the WMO (Maturilli et al.,
272 2013). The settlement at 78.9°N, 11.9°E, is situated on the south coast of the Kongsfjord, which opens at the west coast of
273 Svalbard towards the Fram Strait. The fjord stretches in southeast-northwest direction from the large glacier plateau to the
274 open ocean, and is surrounded by glaciated mountains with altitudes up to 1 km. This geographical setting impacts the local
275 wind field in the lowermost kilometer, resulting in a mainly southeastern wind direction at Ny-Ålesund, which is temporarily
276 replaced by a north-westerly wind direction when large-scale synoptic wind is also coming from the according direction. Only
277 in calm conditions with wind speed $< 2 \text{ m/s}$ do katabatic winds from the glaciers south of Ny-Ålesund prevail.

278
279 Ny-Ålesund experiences monthly temperatures ranging from -8 to 9 °C (annual mean of -6 °C) and average monthly
280 precipitation ranging from 17 to 46 mm (annual total of ~590 mm). Ny-Ålesund may be located in the high Arctic, but due to
281 its location in a coastal environment affected by the West Spitsbergen Current, the local climate is quite maritime and relatively
282 warm. During the summer months, air temperatures above freezing and the otherwise snow-covered landscape exhibits tundra
283 ground and the active layer soil surface of permafrost. An overview of the climate conditions and changes in Svalbard is given
284 by the Norwegian Centre for Climate Services (NCCS, 2018), while the specific atmospheric and radiation conditions in Ny-
285 Ålesund are described by Maturilli et al. (2019).

286
287 ~~The Norwegian Meteorological Institute (aka MET Norway; www.met.no) is operating the standard meteorological surface~~
288 ~~and synoptic observations reported to the WMO.~~ For the YOPP SOPs, the radiosonde launch frequency was increased from
289 daily to 6-hourly. Radiosonde launches, four times daily, are contributed by the Alfred Wegener Institute (AWI), and carried
290 out by the German-French AWIPEV research base that AWI jointly operates with the French Polar Institute Paul-Émile Victor
291 (IPEV). The radiosondes and weekly ozone sondes are launched from a balloon platform about 200m west of the MET Norway
292 weather mast. Atmospheric trace gases and cloud condensation nuclei are observed at the Zeppelin Observatory at about 474
293 m a.s.l. on Zeppelin Mountain south of Ny-Ålesund, operated by the Norwegian Polar Institute (NPI), the Norwegian Institute
294 for Air Research (NILU), Stockholm University, the Japanese National Institute of Polar Research (NIPR), and others. The
295 full complement of atmospheric measurements at Ny-Ålesund highlights the interwoven research community that contributes
296 to making Ny-Ålesund an observational supersite. More information on the Ny-Ålesund Research Station is available at
297 <https://nyalesundresearch.no>.

298 2.7 Eureka, Canada

299 The ~~CA~~nadianCanadian Network for the Detection of Atmospheric Change (CANDAC) runs the Polar Environment
300 Atmospheric Research Laboratory (PEARL) (Figure 8) near the Environment and Climate Change Canada (ECCC) Eureka
301 Weather Station (EWS) in Nunavut, Canada. PEARL has three facilities: the Ridge Laboratory (RL), the Zero Altitude PEARL
302 Auxiliary Laboratory (OPAL), and the Surface and Atmospheric Flux Irradiance Extension (SAFIRE). PEARL collects a wide
303 variety of measurements across all three facilities (Figure 8 and Table 10). The observations used from the Eureka station for
304 the MODF_{ysm} (Akish and Morris, 2023a) were primarily measured at the OPAL and SAFIRE on-site facilities. The OPAL lab
305 is situated at approximately 10 m a.s.l. elevation to capture measurements in the lowermost atmosphere. The SAFIRE facility
306 is located about 5 km from the EWS, and it is located away from any structures. At SAFIRE, there is a former BSRN station,
307 a flux tower, and additional remote sensing instrumentation. ~~and in depth~~Additional details about the site including its
308 instrumentation, dataset validation and uncertainties, etc., can be found in Fogal et al. (2013) and at [https://www.pearl-](https://www.pearl-candac.ca/website/index.php/facilities)
309 [candac.ca/website/index.php/facilities](https://www.pearl-candac.ca/website/index.php/facilities). Only a subset of the available measurements collected have been included in the
310 MODF_{ysm} (Akish ~~&and~~ Morris, 2023a) due to time constraints and processing resources.

311
312 ~~Details of Eureka's climatology are described in Lesins et al. (2010) and water vapor climatology in Weaver et al. (2017). For~~
313 ~~the period from 1954–2007, the monthly average dry-bulb air temperature minimum occurs in February at approximately –37~~
314 ~~°C, with the maximum in July at approximately 5 °C. ECCC also publishes climate normals for Eureka at~~
315 ~~https://climate.weather.gc.ca/climate_normals/results_1981_2010_e.html?stnID=1750&autofwd=1, which for a time period~~
316 ~~of 1981–2010, report a minimum monthly average temperature of –37.4 °C in February and a maximum of 6.1 °C in July.~~

317 ~~Average yearly precipitation is reported as 79.1 mm, with a yearly average snowfall of 60.3 cm and yearly average rainfall of~~
318 ~~32.5 mm. The soils are mostly marine deposits, and the topography, apart from the stony ridges, is driven mostly by ground~~
319 ~~ice (Pollard & Bell, 1998; Pollard et al., 2015). Eureka is generally colder and drier than Utqiagvik (Cox et al., 2012). Cloud~~
320 ~~cover over Eureka is anomalous relative to other Arctic observatories, with generally higher cloud bases, a smaller proportion~~
321 ~~of supercooled liquid, and a seasonal cycle offset from the typical pattern observed elsewhere (Shupe, 2011; Shupe et al.,~~
322 ~~2011). Ellesmere Island, where Eureka is situated, is characterized by complex topography that generates mesoscale~~
323 ~~atmospheric circulations, such as downsloping winds (e.g., Persson and Stone, 2007). The local summertime atmosphere is~~
324 ~~likely regulated also by nearby ice conditions (Persson and Stone, 2007; Tremblay et al., 2019), which vary between the~~
325 ~~northern side of the island where multiyear pack ice persists (e.g., Alert) and other coastal areas, which are generally adjacent~~
326 ~~to seasonal ice cover (e.g., Eureka). However, the general dryness of the atmosphere over Ellesmere is likely a regional~~
327 ~~anomaly related to location relative to dominant pressure patterns over the Beaufort Sea and near the pole rather than being~~
328 ~~local (Cox et al., 2012).~~

330
331 Eureka has a minimum monthly average temperature of -37.4 °C in February, a maximum of 6.1 °C in July, and a yearly
332 average of -19 °C. Average monthly precipitation ranges from 9 to 53 mm (annual total of ~285 mm). Details of Eureka's
333 climatology are described in Lesins et al. (2010) and water vapor climatology in Weaver et al. (2017). For the period from
334 1954–2007, the monthly average dry bulb air temperature minimum occurs in February at approximately -37 °C, with the
335 maximum in July at approximately 5 °C. ECCC also publishes climate normals for Eureka at
336 https://climate.weather.gc.ca/climate_normals/results_1981_2010_e.html?stnID=1750&autofwd=1. Eureka is generally
337 colder and drier than Utqiagvik (Cox et al., 2012). The soils are mostly marine deposits, and the topography, apart from the
338 stony ridges, is driven mostly by ground ice (Pollard and Bell, 1998; Pollard et al., 2015). Cloud cover over Eureka is
339 anomalous relative to other Arctic observatories, with generally higher cloud bases, a smaller proportion of supercooled liquid,
340 and a seasonal cycle offset from the typical pattern observed elsewhere (Shupe, 2011; Shupe et al., 2011). The observations
341 used from the Eureka station for the MODF_{ysm} (Akish & Eureka increased their twice daily radiosonde launches to four daily
342 launches during the SOPs, Morris, 2023a) were primarily measured at the OPAL and SAFIRE on-site facilities. The OPAL lab
343 is situated at approximately 10 m a.s.l. elevation to capture measurements in the lowermost atmosphere. The SAFIRE facility
344 is located about 5 km from the EWS, and it is located away from any structures. At SAFIRE, there is a former BSRN station,
345 a flux tower, and additional remote sensing instrumentation. Eureka increased their twice daily radiosonde launches to four
346 daily launches during the SOPs, specifically in response to a WMO YOPP organizational request.

348 **3 Instrumentation and Derived Variable Calculation**

349 Standard surface meteorological observations (winds, temperature, pressure, humidity, precipitation) were conducted by
350 instruments of similar design, operation, and accuracy at the different sites. The MODF files have an attribute "Instrument,"
351 which specifies the exact instrument model used for each variable at each site. ~~OTT Pluvio2 precipitation weighing gauges,~~
352 ~~which have a quoted precision of ± 0.001 mm and uncertainty $< 5\%$, were deployed at all sites to measure precipitation with~~
353 ~~a single Alter shield configuration (no under catchment corrections were performed; see Section 4). The reported accuracy of~~
354 ~~the Campbell Scientific probes used at some of the sites to measure soil temperature and moisture is 0.3 K and 1.5%,~~
355 ~~respectively. For each site, the full list of measured variables, instrument model and manufacturer, temporal resolution,~~
356 ~~measurement uncertainty, and operating configuration is provided in Tables 4-10 (note that the information in these tables is~~
357 ~~also documented in the attributes of the MODFs themselves). The uncertainties provided in these tables originate from the~~
358 ~~manufacturer and often depend on the meteorological conditions (e.g., relative humidity observations are less accurate during~~
359 ~~very low temperatures); as such, the largest reported uncertainty was provided for each geophysical variable to provide a~~
360 ~~conservative error estimate.~~

361
362 ~~For Whitehorse and Iqaluit, a Vaisala WXT520 was used to measure wind, air temperature, pressure, and relative humidity~~
363 ~~with an accuracy of ± 0.3 m/s, ± 0.3 °C, ± 0.5 hPa, and $\pm 3\%$, respectively. The other sites employed slightly different~~
364 ~~instruments to measure these variables; in general, their reported accuracy is similar or slightly better than the WXT520. Wind~~
365 ~~observations were collected by an RM Young Model 43408/43482/3001 at Utqiaġvik, Tiksi, and Ny Ålesund, a Vaisala~~
366 ~~WAA25 or METEK USA 1 sonic anemometer at Sodankylä, and a Lufft Anemometer at Eureka. Temperature and relative~~
367 ~~humidity observations were collected by Vaisala HMP35D/HMP45D/HMP155/HMT337 sensors in aspirators at Utqiaġvik,~~
368 ~~Tiksi, Sodankylä, Ny Ålesund, and Eureka; they were shielded/housed in the same way. Pressure was obtained from a Vaisala~~
369 ~~PT100/PTB110/PTB220/PTB201 at Utqiaġvik, Tiksi, Ny Ålesund, Sodankylä, and Eureka.~~

370
371 For all sites, Vaisala RS92 or RS41 radiosondes were used to collect vertical profile observations from the surface up to the
372 stratosphere. For Iqaluit and Whitehorse, however, the radiosonde manufacturer changed during SOP2 from Vaisala (RS92)
373 to GRAW on September 12, 2018 (no impact on the data quality is anticipated). ~~These radiosondes have a quoted uncertainty~~
374 ~~of $< \pm 0.5$ °C, 1.0 hPa, 0.15 m/s, and 5% for temperature, pressure, wind, and relative humidity, respectively, in the lower~~
375 ~~atmosphere.~~

376
377 The radiation flux, cloud base height, and snowfall flux observations are the only derived variables that were explicitly
378 calculated in the MODF (as opposed to the direct observations described in the paragraphs above). The ~~radiation~~heat flux
379 observations were processed using the eddy correlation and bulk method (see for instance Baldocchi, 2014). ~~Kipp and Zonen~~
380 ~~pyranometers and pyrgeometers (e.g., CMP22/CNR4/CM11/CMA11/CGR4 models) were used at Iqaluit, Utqiaġvik, and~~

381 ~~Sodankylä, whereas an Eppley PSP pyranometer and PIR pyrgeometer was used at Tiksi, Ny-Ålesund, and Eureka. In general,~~
382 ~~these pyranometers and pyrgeometers have spectral ranges of 200 to 3600 nm (e.g., CMP22) and 4500 to 42000 nm (e.g.,~~
383 ~~CGR4), respectively, a directional error $< \pm 5$ W/m², sensitivity of 5–15 μ V/W/m² and an offset of < 7 W/m² (night time for~~
384 ~~the pyranometer). All upwelling and downwelling, longwave and shortwave radiation measurements were collected at 1-~~
385 ~~minute intervals with instruments in aspirated housing units and no heating elements applied to the instruments. Additional~~
386 ~~processing and quality control~~Additional processing and QC methods for these observations are discussed in Section 4. Cloud-
387 base height observations were output by the Vaisala CL51 ceilometer at most sites (where available) using a proprietary
388 algorithm to determine the lowest cloud base height; the uncertainty of this algorithm isn't reported but the ceilometer has a
389 reported distance accuracy of ± 510 m from the manufacturer. ~~The snowfall flux data was derived from a Ka-band ARM Zenith~~
390 ~~Radar (KAZR) used at the ARM facility, following ARM quality control measures (Widener et al., 2012).~~ ARM technical
391 reports, instrument validation / evaluation, and ~~quality control~~QC measures are linked and available within the
392 Utqiagvik/Barrow MODF_{ysm} (Akish ~~&~~and Morris, 2023c).

393
394 For all observations, instantaneous time is reported at the instruments' raw sampling cadence in UTC. The typical temporal
395 cadence for most observations are around 1 minute ~~or less~~. No temporal interpolation or averaging was performed on the data.
396 The only exception to this is for turbulent fluxes (the only calculated variable), where some averaging (1 to 30 minutes,
397 depending on the variable) is implicit in the calculation of fluxes. Heights are reported as above ground level (AGL), with the
398 exception of the soil thermistor string, which reports depths below the surface in units of cm. ~~Note that the uncertainties~~
399 ~~provided in this Section originate from the manufacturer and often depend on the meteorological conditions (e.g., relative~~
400 ~~humidity observations are less accurate during very low temperatures); as such, the largest reported uncertainty was provided~~
401 ~~for each geophysical variable in order to provide a conservative error estimate.~~ For more information on the instrumentation
402 used or further details on the instrument accuracy, precision, and co-located validation studies for certain instruments, refer to
403 the site-specific references listed in Section 2 and/or the WMO Guide to Instruments and Methods of Observation (WMO,
404 2021).

406 **4 Dataset Preparation, quality control, and post-processing**

407 Guidelines for creating MODFs were published as a table in both human-readable (PDF file) and machine-readable (JSON
408 files) formats by Hartten and Khalsa (2022). This "H-K Table" adopts the standards and conventions commonly used in the
409 earth sciences, including NetCDF encoding with Climate and Forecast (CF) Conventions and following ~~CMIP6~~CMIP6
410 naming, as agreed upon by the YOPP community (Uttal et al., ~~2023~~2024). This H-K standard facilitates the creation of MODFs
411 using current requirements and the creator's software of choice, with the MODF toolkits providing tools to assist the user in

412 creating MODFs (Section 6). For the present work, we used H-K Table version 1.3 to guide the criteria for the generation and
413 standardization of naming conventions, units, and global/variable attribute metadata. Observational datasets were collated and
414 formatted for each of the seven ~~supersites~~ sites into a set of NetCDF files in accordance with the table’s criteria. The native
415 variable name is saved as an attribute in the MODFs and as previously discussed, no resampling was performed to harmonize
416 different time stepping (the instrument’s instantaneous raw sampling frequency is reported, usually about minutely).
417 Acceptance of data into the MODF_{ysm} was generally determined by the variable list described in the table. The processing
418 script is openly available and described in Section 6.

419
420 Radiosonde (timeSeriesProfileSonde variables) data in the MODF were binned into 5-meter intervals (10 m for Iqaluit and
421 Whitehorse) of geopotential height and all measurements within each bin were averaged. The raw data feed from the
422 radiosonde observations were obtained at ~2 s resolution. In the case of 5-meter intervals, this most often results in 0, 1, or 2
423 measurements in each bin: 8%, 82%, 9%, respectively, in SOP1 and 6%, 80%, 13% in SOP2. In both SOP1 and SOP2
424 at least 99.9% of the measurements have 2 or fewer measurements, but a given bin can have up to 14 measurements. The
425 number of measurements per bin has been included in the dataset to filter for these situations, as have the actual time and
426 height of each measurement (though also averaged within each bin). For surface precipitation observations, no corrections for
427 solid precipitation under-catchment were performed (the dataset is raw in the MODF); where appropriate, users are
428 recommended to process under-catchment corrections via Kochendorfer et al. (2020).

429
430 ~~The principal goal of the present phase of the MODF concept is to standardize~~ A summary of the instruments, their
431 configuration, processing, and QC applied for each site’s observations is provided in Tables 4-10. Unless otherwise specified
432 in these Tables, the observations collected by each instrument are processed by the instrument manufacturers’ proprietary
433 software (standard data output for that instrument) prior to any additional QC performed. In some cases, no additional QC was
434 performed, and the data should be treated “as is.” In other cases, additional checks (manual comparisons to co-located
435 instruments) and/or QC was applied to remove outliers and erroneous observations, as described under ‘Quality Control’ in
436 Tables 4-10. An indication of whether the dataset was corrected for certain effects (e.g., shelter heating effect) is also provided
437 in the Tables, where applicable.

438 The present phase of the MODF concept is to use standardized data organization, metadata, and interoperability. While data
439 quality assurance and measurement operation procedures remain in the purview of the contributing stations, considerable effort
440 was undertaken to ensure MODF production followed a transparent, consistent, and standardized data processing chain. This
441 includes efforts to standardize post-processing and filtering techniques (e.g., ~~quality control~~ QC methods) as much as possible
442 for the same geophysical variable across the different sites. This consistent processing chain is another unique feature of the
443 MODF dataset as it enforces a level of consistency across vastly different observation sites that normally follow their agencies’
444 own data production procedures and methods. ~~As identified~~ As discussed in more detail in the below subsections, there are

445 some cases where site-specific data processing could not be avoided; data should be used cautiously and with due consideration
446 to each ~~supersite's site's~~ processing techniques and ~~quality-control~~(QC) methods for the MODF_{ysm}.

447 4. 1 Whitehorse and Iqaluit, Canada

448 All geophysical variables observed at the Iqaluit and Whitehorse sites were processed in the same manner and included in the
449 MODF_{ysm} (Huang et al., ~~2023a; 2023b; 2023a~~). For most geophysical variables, limited QC was performed on the raw dataset
450 with the intention to remove obvious outliers only. ~~Surface variables were checked against climatology ranges and the rate of~~
451 ~~change thresholds, which were based on hourly criteria. Details regarding the QC performed are provided in Tables 4-5.~~ A very
452 small number (<5%) of observations were flagged by the QC algorithm. ~~Note that the correction for solid precipitation under-~~
453 ~~catchment is less relevant for the WXT520 instrument than it is for traditional precipitation rain gauge instruments (e.g., the~~
454 ~~Pluvio2).~~ The radiation flux observations should be treated with caution since they typically require additional QC processing
455 prior to analysis; no additional QC was performed on these observations to account for potential frost or snow deposition on
456 the sensors, for instance. No additional QC was performed on the cloud base height data, which was processed by the Vaisala
457 software. Vaisala also processed the raw data feed from the radiosonde observations, which was obtained at 2 s resolution; no
458 additional QC was performed. ~~-~~When no data was available (due to the instrument being down, loss of power at the site, or
459 because it was flagged by the QC algorithm), a missing value (-9999.0) was reported in the MODF_{ysm} (Huang et al., 2023a;
460 2023b) and is notated via the "missing_value" attribute associated with each variable. Mariani et al. (2020, 2021) provides
461 instrument validation studies and more detailed information on the ~~quality-control~~QC processing routines for the remote
462 sensing and upper air observations.

463 4. 2 Sodankylä, Finland

464 The Sodankylä observations included in the MODF_{ysm} (O'Connor, 2023) are automatically uploaded every day to the FMI
465 open access web site <https://litdb.fmi.fi/> where the data are organized on the basis of platforms and stations. Before being
466 uploaded to the web page, the data undergo an automatic quality check to remove outliers, ~~as described in Table 6. In several~~
467 ~~cases, multiple different instruments were co-located and deployed at the site to observe the same variable; as such there are~~
468 ~~multiple sources of observations (instruments) to choose from.~~

469
470 In the current MODF_{ysm} version (O'Connor, 2023), no further quality check was applied to the data, implying that errors from
471 several sources ~~(such as are occasionally included. These sources of error may include~~ snow/frost deposition on radiation and
472 temperature sensors or absorption of solar radiation by unsheltered temperature sensors) ~~are occasionally included.~~ In a future
473 version of the MODF_{ysm}, a deeper quality check will be applied to some of the variables included in the current MODF_{ysm}

Formatted: Space After: 12 pt

Formatted: Not Highlight

474 (O'Connor, 2023). This quality check is based on the comparison among the same variables measured at different sites, on
475 visual inspection and, in the case of global radiation, on the comparison with radiative transfer model calculations. This
476 processing will enable the identification of the shortwave data affected by the shadows casted by the vegetation, of errors
477 caused by frost formation on the domes of pyranometers, and of the error in unshaded thermometers caused by the absorption
478 of solar radiation. ~~As in the case of the Eureka observatory, the radiosonde data in the MODF was ingested and processed by~~
479 ~~IGRA and is available through NOAA's NCEI portal (Durre et al., 2018).~~

480 **4.3 Utqiaġvik (formerly barrow), USA, Tiksi, Russia and Eureka, Canada**

481 The Utqiaġvik/Barrow data within the MODF_{ysm} (Akish ~~&~~and Morris, 2023c) originated from both ~~Atmospheric Radiation~~
482 ~~Measurement (DOE/ARM) and the Global Monitoring Laboratory (and NOAA GML)~~ datasets, with GML proving datasets
483 for ozone, snow thickness, skin temperature, soil temperature profile. Value added products were generated and disseminated
484 to the users using the ARM Data Discovery interface. Both the ARM and GML datasets were ingested into a single MODF_{ysm}
485 with variable attribution detailing how each variable and data set was ~~quality-controlled~~QC'd, processed and accessed. ~~As~~
486 ~~described in Tables 7-8, 10.~~ The surface ozone data was collected in 1-minute intervals and was manually ~~quality~~
487 ~~controlled~~QC'd and submitted to NCEI.

488
489 The measurements collected by the ARM facility were processed, QC analyzed, and archived at the ARM Data Center archive.
490 The long-term Eureka and Tiksi datasets (flux tower and radiation) are hosted by the NOAA Physical Sciences Laboratory
491 (PSL), in collaboration with ECCO (Eureka site only), and Roshydromet (Tiksi site only).

492
493 ~~For The~~the three sites, the radiation measurements were QC'd and processed following Long ~~&~~and Shi (2008). ~~Heat) and~~
494 ~~improved correction of the infrared loss in diffuse shortwave measurements was included (Younkina and Long, 2003).~~
495 ~~Turbulent heat~~ fluxes were processed and QC'd via Eddy correlation corrections including stability correction, Webb-Pearman
496 correction, frequency correction, sensor separation correction, filtering correction, line-averaging correction, and volume-
497 averaging correction (Cook et al. 2008, Fuehrer and Friehe 2002). Bulk corrections were also employed and utilized ARM
498 data from the radiation, ground, met, and tower.

499
500 Radiosonde data were ingested and processed by NOAA's NCEI and was processed through IGRA, following their standards
501 (Durre et al., 2018) and is available through NOAA's NCEI portal. The IGRA 2 QA system processed the sonde data, which
502 is based largely on the QA procedures in the IGRA 1 system (Durre et al. 2006; Durre et al. 2008). Like the IGRA 1 system,
503 it consists of a deliberate sequence of specialized algorithms, each of which makes a binary decision on the quality of a value,
504 level, or sounding; either the data item passes the check and remains available, or it is identified as erroneous and thus set to

505 missing. For all ~~other observations' QC observations~~, a ~~first-level automated QC was established by climatological ranges in the~~
506 ~~same way as for Whitehorse and Iqaluit~~. A second level of manual QC was performed whereby data was reviewed by
507 instrument mentors and visually assessed by the site scientist/data quality office.

508 **4.4 Tiksi, Russia and Eureka, Canada**

509 ~~Data collection and processing techniques for Eureka are the same as for the Tiksi site. The long-term Eureka and Tiksi datasets~~
510 ~~(flux tower and radiation) are hosted by the NOAA Physical Sciences Laboratory (PSL), in collaboration with ECCO (Eureka~~
511 ~~site only), and Roshydromet (Tiksi site only). All meteorological measurements within the MODF_{ysm} (Akish & Morris, 2023b),~~
512 ~~i.e., air temperature, skin temperature, soil temperature, snow thickness, pressure, relative humidity, wind speed and direction,~~
513 ~~were manually quality controlled first via an automated QC established by climatological ranges in the same way as for~~
514 ~~Whitehorse et al. Following this, a manual/visual inspection was performed. This included removing non-physical values and~~
515 ~~outliers, after confirming that they were either biased, incorrect, or collected during site maintenance periods. The radiation~~
516 ~~measurements were validated and processed using the Long QCrad method (Long & Shi, 2008) and improved correction of~~
517 ~~the infrared loss in diffuse shortwave measurements (Younkin & Long, 2004), and again, were visually inspected. The~~
518 ~~radiosonde dataset was processed through IGRA's processing techniques and is based on the QC procedures in the IGRA 1~~
519 ~~system (Durre et al., 2006; Durre et al., 2008). If data was not available for any of the collected measurements across any of~~
520 ~~the variables, due to the instrument being down, loss of power at the site, or because it was flagged by the QC algorithm, a~~
521 ~~missing value (-9999) was reported in the MODF_{ysm} (Akish & Morris, 2023b).~~

Formatted: Font color: Custom Color(34,34,34)

522 **4.5 Ny-Ålesund, Norway**

523 The meteorological measurements used for the MODF_{ysm} (Holt, 2023) are taken from the AWIPEV weather mast (Driemel et
524 al., 2018; Maturilli, 2020b). Except for precipitation, all other data used in the MODF_{ysm} for Ny-Ålesund originated from the
525 following data sets: Maturilli (2020a, 2020b, 2020c, 2022). The precipitation data reported in the MODF_{ysm} are the direct
526 instrument output and no quality checks were applied; as such this data should be treated with caution (Holt, 2023). The Ny-
527 Ålesund observations included in the MODF_{ysm} are a subset of those regularly uploaded in the PANGAEA data repository
528 (www.pangaea.de). Before being uploaded, all data undergo an automatic quality check ~~established by climatological~~
529 ~~ranges (described in the same way as for Whitehorse et al. Table 9)~~. Following this, additional manual/visual inspection was
530 performed ~~accounting for e.g., physical plausibility as for Utqiaġvik, Tiksi, and Eureka~~. Surface radiation data were validated
531 and have undergone all quality checks of BSRN before archiving (Maturilli, 2020a). ~~Automated QC was performed on the~~
532 ~~radiosonde data, established by climatological norms; a second level of data was reviewed by the instrument mentor before~~
533 ~~storing the data at the PANGAEA repository.~~

534

535 **5 MODF Data Structure**

536 The data inside a MODF comprises of all the observations listed in Table 3 for a given observation site. The data itself follows
537 the same standardized format and structure for all observations and sites and is stored into a single NetCDF file using CF
538 conventions. NetCDF file formatting was chosen to best accommodate the high-level of metadata detail required for merging
539 such large quantities of individual measurements together, particularly given the need to be as transparent as possible when
540 reporting instrument-specific details for each observation. [NWP model output was stored in MMDFs, matching the MODF
541 format to facilitate model-observation comparisons. Local maps showing the synoptic region around each site are provided in
542 Figure 9, with native spatial grids of the forecast models that participated in YOPPSiteMIP overlaid. This provides visual
543 context of where the site and the nearest NWP grid points exist in and around each site.](#)

544
545 All MODF_{ysm} measurements provided in the data files maintained their native time cadence (typically on the order of minutely)
546 with no averaging undertaken, and details of the collection and processing techniques can be found in the variable attributes
547 within the files. Each DOI in Table 2 contains four (e.g., Whitehorse) or six (e.g., Utqiagvik) files, depending on whether the
548 site had timeSeriesProfile observations on a tower/mast. The filename convention for each MODF is as follows: site name +
549 “obs” + MODF_featureType + start_date + end_date.nc.

550
551 Guidelines for creating inventories of variable and attribute information (metadata) necessary for the MODF file attributes
552 were published in spreadsheet format by Morris and Akish (2022). This “A-M Template” uses variable content criteria from
553 the H-K Table to generate a metadata matrix of attribute and variable information for each of the measurements contained
554 within the MODFs. The template has individual tabs for each of the corresponding CF metadata featureTypes (i.e., timeSeries
555 and timeSeriesProfile) of the MODF NetCDF files, as well as one tab for the Global Attributes of the MODFs. The CF
556 Conventions can be found here: <https://cfconventions.org/cf-conventions/cf-conventions.html>. The attributes within the
557 template are mandatory when applicable, and serve as a guideline for MODF creators. The A-M Template is machine-readable
558 and can be ingested into MODF software to create the final output.

559
560 The file content is well-illustrated in Table 3; other details of the MODF_{ysm} format and structure are outlined in Uttal et al.
561 (20232024). MODFs can contain featureTypes such as timeSeries and timeSeriesProfile, which refer to time series having one
562 and two data dimensions, respectively. In cases where data subcategories exist, featureType modifications can be depicted in
563 the file name, for example timeSeriesProfileSonde exist for the MODF_{ysm}. Currently, more than one featureType can be used
564 within an individual MODF file, but all subscribe to the same formatting structure and nomenclature. To generate an MODF,

565 creators would first visit the H-K Table to determine the variables that will be included in their MODF, and then they should
566 utilize the A-M Template to fill in the needed attribute and variables information requested by existing MODF software. Once
567 the A-M Template has been completed, then users can ingest the template into their MODF software to create the final MODF
568 outputs. For the MODF_{ysm}, individual toolkits were developed by MODF makers for each YOPP [supersite](#). Python code
569 was developed for Whitehorse, Iqaluit and Ny-Alesund, and MATLAB code for Utqiagvik, Tiksi, Eureka and Soldankyla (see
570 Section 6). After the generation of the MODF_{ysm} outputs, the files were run through an MODF checker that identifies the
571 various inconsistencies or issues with the files before their upload to the MET Norway data portal. The MODF_{ysm} checker
572 developed for the YOPPsiteMIP files is part of a larger toolkit being designed to continue the creation of MODFs.

573
574 As an example of the uniformity of the observations (in terms of data format, post-processing, temporal cadence, etc.)
575 contained within each [supersite's](#) MODF_{ysm} and their [excellent](#) data coverage during the two YOPP SOPs, Figures [310](#)
576 and [411](#) provide the surface downwelling longwave radiation and near-surface temperature observations from each
577 [supersite's](#) MODF_{ysm} during SOP1, respectively and Figures [512](#) and [613](#) show the same except for SOP2. The MET
578 Norway data portal and MODF maker toolkit (Sect. 6) also provides plotting tools that work with any MODF or MMDF and
579 can produce similar figures automatically. Periods of interest can be quickly identified by users and analyzed for further
580 investigation and/or comparison with their corresponding MMDFs. MODFs significantly simplify the process of analyzing
581 observations from multiple sites and multiple instruments, as analyses and Figures can be produced for each site using a single
582 code that works for any observed geophysical variable and (if desired) their corresponding NWP model output in the MMDF.
583 In contrast, without MODFs a user would have to contact each meteorological agency individually, find each sites' data
584 repository, obtain data access privileges, find the files they need from multiple instruments, reprocess and reformat multiple
585 uniquely-formatted datasets and file types, then develop several different codes (e.g., readers) specific to each instruments'
586 dataset to ingest the multi-variate datasets and plot them.

587
588 The MODF_{ysm} at Sodankylä are unique in that their measurements are collected across a series of sub-sites in the area;
589 therefore, it is important to describe here the possible methods for extracting the data for specific locations, or for co-located
590 measurements. The Sodankylä station comprises at least 25 distinct locations, the precise number of which is given by the
591 dimension 'site_id' inside the MODF data file. Each distinct location is given a unique index key in the variable 'subsite_name',
592 with these indices also identifying the 'lat', 'lon' and 'soil_type' for each location. The corresponding FMI names for each
593 location are identified in the attribute 'flag_meanings' for the variable 'subsite_name' via their indices; for example, the index
594 value of 16 pointing to IOA003_spot_8, which is one of the automatic weather stations located in the Intensive Observations
595 Area (IOA). There may be multiple locations providing the same measurement. However, not all locations provide the same
596 set of measurements, and to keep the MODF compact, each measurement variable has the location dimension truncated to
597 include only locations which measure that variable; i.e., the location dimension for the measurement variables is 'nsubsites_X',

598 where X is the number of locations making the particular measurement. This set of locations is accessed through the indices
599 given in the attribute 'subsite_name' for the measurement variable, which corresponds to the key given in the 'subsite_name'
600 variable; i.e., a subsite_name attribute of "1, 3, 10" means that these measurements were made at the locations identified by
601 their indices, from which their locations (latitudes and longitudes) and soil_type can also be determined.

602

603 This method permits diverse options of collecting measurements for particular uses. All measurements, for example, at one
604 location can be obtained by identifying the appropriate 'subsite_name' index inside the MODF data file, iterating through the
605 'subsite_name' attribute of each variable to see if it contains the selected index, and, if so, selecting the column or slice of data
606 for the data that matches the location of the index (i.e. if subsite_name = 10 and the subsite_name attribute for a timeSeries
607 variable is "1, 3, 10", the measurement timeSeries for the requested location is in the third column, the next variable may have
608 a subsite_name attribute of "1, 3, 5, 6, 10" and the measurement timeSeries for the requested location is in the fifth column).
609 The user could also select a specific area of interest and identify all measurements made within this region as follows: select
610 the indices for the locations within a specified latitude and longitude range, then iterate through the 'subsite_name' attribute of
611 each variable to see if it contains the selected indices and return the columns or slices that match them.

612

613 Note that each [supersitesite](#) conducts additional observations not listed in table 3 that will be included in upcoming updates to
614 the MODF_{ysm} with the intent to eventually incorporate all observations into the MODF_{ysm} for each [supersitesite](#). This process
615 of developing and appending to MODFs can be extended to other sites and/or research programs that wish to create MODFs
616 of their observations. Given the standardized nature of the MODFs, reading and analyzing datasets from any of the YOPP
617 [supersitesites](#) is simplified. Quick-look plotting tools have been developed via the MET Norway YOPP data portal and the
618 MODF maker toolkit (Sect. 6), which enable near-instantaneous plotting of the observations contained within the MODF_{ysm}.

619

620 **6 Data and Code Availability**

621 The MODF_{ysm} for each [supersitesite](#) are available via the MET Norway YOPP Data Portal (<https://yopp.met.no/>) where they
622 are indexed through FAIR compliant discovery metadata and can be directly accessed at:

623 https://thredds.met.no/thredds/catalog/alertness/YOPP_supersite/obs/catalog.html (Whitehorse:

624 <https://doi.org/10.21343/a33e-j150>, Iqaluit: <https://doi.org/10.21343/yrnf-ck57>, Sodankylä: <https://doi.org/10.21343/m16p->

625 [pq17](https://doi.org/10.21343/a2dx-nq55), Utqiagvik: <https://doi.org/10.21343/a2dx-nq55>, Tiksi: <https://doi.org/10.21343/5bwn-w881>, Ny-Ålesund:

626 <https://doi.org/10.21343/y89m-6393>, Eureka: <https://doi.org/10.21343/r85j-tc61>).

627

628 Proper data citation ensures appropriate credits to authors of both input data sources and merged MODF_{ysm} datasets. Data from
629 each station has been assigned a DOI. The variable attributes of the merged data products contain information about the source
630 datastreams and their DOIs, to more clearly establish data provenance in a traceable manner. When using data from the
631 MODF_{yms} , it is expected that the user references the MODF_{ysm} DOI, and any subsidiary variable DOIs when available.
632 Assigning citations for merged data streams such as the MODF_{ysm} is a challenging and still evolving concept. For example,
633 the US ~~Department of Energy (DOE)-Atmospheric Radiation Measurement (ARM)~~ Program uses a combination of DOI and
634 citation structure for continuous data streams, as outlined in Prakash et al. (2016). They recommend when registering DOIs
635 for derived and higher-order data, source DOIs in the metadata of the newly created DOI should be added and linked when
636 possible.

637
638 The source code used to produce the MODF_{ysm} for each [supersitesite](#) (and MODFs in general) are available via gitlab:
639 <https://gitlab.com/mdf-makers/mdf-toolkit>. This MODF toolkit is openly available for anyone interested in developing their
640 own MODF file or generating quick-look plots of the data contents inside the MODFs. The toolkit is regularly updated as the
641 MODF community grows and new geophysical variables and/or functions are added. Additional site-specific python and
642 MATLAB codes that were used to prepare the observation data files for MODF ingestion are available upon request (e.g.,
643 contact the site principle investigator).

645 7 Concluding Remarks

646 The enhanced ground-based observations conducted at both Poles during the YOPP fill significant and identified gaps in our
647 current meteorological observation capabilities for the Polar Regions. YOPPsiteMIP MODFs (MODF_{ysm}) have been published
648 for seven of the YOPP Arctic [supersitesites](#), whereby all geophysical variables are stored in an identical, standardized format
649 in a single NetCDF file following CF conventions, ~~fulfilling~~. [This fulfills](#) a key objective of the program to perform single- or
650 multi-variate model-observation comparisons. These MODFs archive data in a manner as similar as possible to corresponding
651 MMDF (see Uttal et al., [20232024](#)) that contain high-resolution forecast variables from a single NWP model at and around a
652 [supersitesite](#) (Figure 29). Thus, combined, MODFs and MMDFs greatly simplify integration of these complex datasets,
653 enabling further scientific study as demonstrated in the recent publications using the latest MODF_{ysm} and MMDF_{ysm} (Day et
654 al., [20232024](#)).

655
656 Standardized geophysical variable nomenclature, cadences, metadata, basic QC, and file structure were employed to create
657 these files. MODFs provide the first standardized files for archiving all the different ground-based observation [supersitesite](#)
658 observations, containing a multitude of geophysical variables observed by (at times) different instruments. This amalgamation

659 of different sites' observations into a standardized, user-friendly MODF format enables easier analysis of the MODF dataset,
660 inter-site comparisons, and detailed NWP model validation, evaluation, intercomparisons, and process-based diagnostic
661 studies that are currently underway ([see.g., Figures 3-10 to 6-as-an-example13](#)). The further adoption, creation, and use of
662 MODFs outside of YOPP is encouraged; a suite of tools and documentation is openly available via Gitlab ([see](#)-Sect. 6) for
663 other site managers, researchers, and users to develop and create their own site-specific MODFs outside of YOPP or to analyze
664 an observation sites' dataset.

665
666 The YOPP MODF_{ysm} discussed here provide novel access to datasets of enhanced meteorological observations collected at
667 several [supersites](#) across the Arctic. The MODF concept is not limited for use in polar regions and could be exported
668 elsewhere. Seven YOPP-designated [supersites](#) in the Arctic developed and published MODF_{ysm} covering both SOP periods
669 (February – March 2018 and July – September 2018), including Iqaluit, Whitehorse, and Eureka in Canada, Utqiagvik in the
670 United States, Tiksi in Russia, Sodankylä in Finland, and Ny-Ålesund in Norway. Additional geophysical variables observed
671 at each of these seven [supersites](#) will be included in a future update of their MODF_{ysm}, with the goal of having [100%almost](#)
672 [all](#) of a site's observations available. Observations at most of these sites continue today beyond YOPP and are available for
673 subsequent analyses, in some cases using updated MODFs generated in near-real time. MODF_{ysm} for the other YOPP sites,
674 including ship-based platforms and [supersites](#) in the Antarctic, will be made available in the future to complete the YOPP
675 dataset. The MODF_{ysm} described here directly ties to process-oriented verification studies aiming to improve NWP predictions
676 at the Poles by contributing and enabling NWP inter-comparisons.

677

678 **Author contributions**

679 SM, ZM, and TU wrote the first draft of the manuscript. SM and ZM conducted scientific analyses and created tables and
680 figures with JD and JT. All authors managed data archiving, creation of the MODF_{ysm}, and publication to the MET Norway
681 YOPP Data Portal. All authors contributed to the writing and the editing of the manuscript.

682

683 **Competing interests**

684 The authors declare that they have no conflict of interest.

685

686 **Disclaimer**

687 Use of specific instrument manufacturers/models and suppliers mentioned in the manuscript and/or used at the
688 [supersites](#) is not a commercial endorsement of their products.

689

690 **Acknowledgements**

691 This is a contribution to the Year of Polar Prediction (YOPP), a flagship activity of the Polar Prediction Project (PPP), initiated
692 by the World Weather Research Programme (WWRP) of the World Meteorological Organisation (WMO). We acknowledge
693 the WMO WWRP for its role in coordinating this international research activity. This study was supported by NOAA's Global
694 Ocean Monitoring and Observing Program through the Arctic Research Program (FundRef:
695 <https://doi.org/10.13039/100018302>)-<https://doi.org/10.13039/100018302>). Special thanks to the station technicians and
696 operators at the [supersites](#) for deploying instruments, maintenance, and technical services. In particular, thank you to the
697 radiosonde operators for providing extra daily sonde launches during the two SOP periods. Thank you to Jenn Glaser for her
698 contract work in creating the station graphic in Figure 1, and to Kyrie Newby and Calvin Jesse for [updating](#) [creating](#) the Google
699 Earth images in Figure 29. JD was supported by the European Union funded INTERACTIII project (Grant Agreement:
700 871120). AK and LMH were supported in part by NOAA cooperative agreements NA17OAR4320101 and
701 NA22OAR4320151. Portions of the MODF_{ysm} data were obtained from the Atmospheric Radiation Measurement (ARM) user
702 facility, a U.S. Department of Energy (DOE) office of science user facility managed by the biological and environmental
703 research program. Thank you to MET Norway for hosting the YOPP data portal. All data products are produced by their
704 respective institutions and are available via the YOPP data portal (<https://yopp.met.no>) and directly at
705 https://thredds.met.no/thredds/catalog/alertness/YOPP_supersite/obs/catalog.html.
706
707

708 **References**

- 709 Akish, E., & Morris, S.: MODF for Eureka, Canada, during YOPP SOP1 and SOP2, Norwegian Meteorological Institute,
710 [dataset, https://doi.org/10.21343/R85J-TC61](https://doi.org/10.21343/R85J-TC61), 2023a.
- 711
- 712 Akish, E., & Morris, S.: MODF for Tiksi, Russia, during YOPP SOP1 and SOP2, Norwegian Meteorological Institute,
713 [dataset, https://doi.org/10.21343/SBWN-W881](https://doi.org/10.21343/SBWN-W881), 2023b.
- 714
- 715 Akish, E., & Morris, S.: MODF for Utqiagvik, Alaska, during YOPP SOP1 and SOP2, Norwegian Meteorological
716 Institute, [dataset, https://doi.org/10.21343/A2DX-NQ55](https://doi.org/10.21343/A2DX-NQ55), 2023c.
- 717
- 718 Baldocchi, D.: Measuring fluxes of trace gases and energy between ecosystems and the atmosphere – the state and future of
719 the eddy covariance method. *Global Change Biology* (2014)20, 3600–3609, <https://doi.org/10.1111/gcb.12649>, 2014.
- 720
- 721 [Becherini, F., Vitale, V., Lupi, A. et al. Surface albedo and spring snow melt variations at Ny-Ålesund, Svalbard. *Bull. of*
722 *Atmos. Sci. & Technol.* 2, 14 \(2021\). <https://doi.org/10.1007/s42865-021-00043-8>.](https://doi.org/10.1007/s42865-021-00043-8)
- 723
- 724 Cassano, J. J., Higgins, M. E., and Seefeldt, M. W.: Performance of the Weather Research and Forecasting Model for
725 Month-Long Pan-Arctic Simulations, *Monthly Weather Review*, 139, 3469–3488, [doi: 10.1175/mwr-d-10-05065.1](https://doi.org/10.1175/mwr-d-10-05065.1), 2011.
- 726
- 727 Cohen, J., Rautiainen, K., Lemmetyinen, J., Smolander, T., Vehvilainen, J., and Pulliainen, J.: Sentinel-1 based soil
728 freeze/thaw estimation in boreal forest environments, *Remote Sens Environ*, 254, [ARTN
112267https://doi.org/10.1016/j.rse.2020.112267](https://doi.org/10.1016/j.rse.2020.112267), 2021.
- 729 [10.1016/j.rse.2020.112267](https://doi.org/10.1016/j.rse.2020.112267), 2021.
- 730
- 731
- 732 [Cook, B.I., Bonan, G.B., Levis, S. et al. The thermoinsulation effect of snow cover within a climate model. *Clim Dyn* 31,
733 107–124. <https://doi.org/10.1007/s00382-007-0341-y>, 2008.](https://doi.org/10.1007/s00382-007-0341-y)
- 734
- 735 Cox, C.J., Stone, R.S., Douglas, D.C., Stanitski, D.M., Divoky, G.J., Dutton, E.S., Sweeney, C., George, J.C., and
736 Longenecker, D.U.: Drivers and Environmental Responses to the Changing Annual Snow Cycle of Northern Alaska, *B Am*
737 *Meteorol Soc*, 98, 2559–2577, <https://doi.org/10.1175/BAMS-D-16-0201.1>, 2017.
- 738
- 739 Cox, C.J., Walden, V.P., and Rowe, P.M.: A Comparison of the atmospheric conditions at Eureka, Canada, and Barrow,
740 Alaska (2006–2008), *J Geophys Res*, 117, <https://doi.org/10.1029/2011JD017164>, 2012.
- 741
- 742 Day, J.J., Sandu, I., Magnusson, L., Rodwell, M.J., Lawrence, H., Bormann, N., and Jung, T.: Increased Arctic influence on
743 the midlatitude flow during Scandinavian Blocking episodes, *Q.J.R. Meteorol. Soc.*, 725, 3846–3862,
744 <https://doi.org/10.1002/qj.3673>, 2019.
- 745
- 746 Day, J., Svensson, G., Casati, B., Uttal, T., Khalsa, S.J., Bazile, E., Akish, E., Azouz, N., Ferrighi, L., Frank, H., Gallagher,
747 M., Godoy, Ø., Hartten, L., Huang, L., Holt, J., Di Stefano, M., Mariani, Z., Morris, S., O’Connor, E., Pirazzini, R., Remes,
748 T., Fadeev, R., Solomon, A., Tjerström, J., and Tolstykh, M.: The YOPP site Model Intercomparison Project (YOPPsiteMIP)
749 phase 1: project overview and Arctic winter forecast evaluation, [20232024](https://doi.org/10.21957/2023-2024), *submitted to Geoscientific Model Development*
750 *(GMD) August 25, 2023 –submitted - under review 2024*.

Formatted: Font color: Blue

Formatted: Font color: Blue

Formatted: Font color: Blue

Formatted: Font color: Blue

751
752 Driemel A, Augustine JA, Behrens K, Colle S, Cox C, Cuevas-Agulló E, Denn FM, Duprat T, Fukuda M, Grobe H,
753 Haeffelin M, Hyett N, Ijima O, Kallis A, Knap W, Kustov V, Long CN, Longenecker D, Lupi A, Maturilli M, Mimouni M,
754 Ntsangwane L, Ogihara H, Olano X, Olefs M, Omori M, Passamani L, Pereira EB, Schmithüsen H, Schumacher S, Sieger R,
755 Tamlyn J, Vogt R, Vuilleumier L, Xia X, O A, König-Langlo G. Baseline Surface Radiation Network (BSRN): structure and
756 data description (1992–2017) *Earth Syst Sci Data*, 10, 1491–1501, 2018.

757
758 Durre, I., Menne, M. J., and Vose, R. S.: Strategies for evaluating quality assurance procedures, *J Appl Meteorol Clim*, 47,
759 1785-1791, [doi:10.1175/2007jamc1706.1](https://doi.org/10.1175/2007jamc1706.1), 2008.

760
761 Durre, I., Vose, R. S., and Wuertz, D. B.: Overview of the Integrated Global Radiosonde Archive, *J Climate*, 19, 53-68,
762 [doi:10.1175/Jcli3594.1](https://doi.org/10.1175/Jcli3594.1), 2006.

763
764 Durre, I., Yin, X., Vose, R. S., Applequist, S., and Arnfield, J.: Enhancing the Data Coverage in the Integrated Global
765 Radiosonde Archive. *J. Atmos. Oceanic Technol.*, 35, 1753–1770, <https://doi.org/10.1175/JTECH-D-17-0223.1>, 2018.

766
767 Fogal, P. F., LeBlanc, L. M., and Drummond, J. R.: The Polar Environment Atmospheric Research Laboratory (PEARL):
768 Sounding the Atmosphere at 80 degrees North, Arctic, 66, 377-386, 2013.

769
770 [Fuehrer, P.L., Friehe, C.A. Flux Corrections Revisited. *Boundary-Layer Meteorology* 102, 415–458.](https://doi.org/10.1023/A:1013826900579)
771 <https://doi.org/10.1023/A:1013826900579>, 2002.

772
773 Gallagher & Tjernström: Accelerating research in weather prediction and model improvement with new free community
774 open source software tools. To be submitted, 2024.

775
776 Goessling, H. F., Jung, T., Klebe, S., Baeseman, J., Bauer, P., Chen, P., Chevallier, M., Dole, R., Gordon, N., Ruti, P.,
777 Bradley, A., Bromwich, D. H., Casati, B., Chechin, D., Day, J. J., Massonnet, F., Mills, B., Renfrew, I., Smith, G., and
778 Tatusko, R.: Paving the Way for the Year of Polar Prediction, *B Am Meteorol Soc*, 97, Es85-Es88, [doi:10.1175/Bams-D-](https://doi.org/10.1175/Bams-D-15-00270.1)
779 [15-00270.1](https://doi.org/10.1175/Bams-D-15-00270.1), 2016.

780
781 [Gordon, M., Biswas, S., Taylor, P. A., Hanesiak, J., Albarran-Melzer, M., and Fargey, S.: Measurements of Drifting and](https://doi.org/10.3137/Ao1105.2010)
782 [Blowing Snow at Iqaluit, Nunavut, Canada during the STAR Project, *Atmos Ocean*, 48, 81–100, 10.3137/Ao1105.2010,](https://doi.org/10.3137/Ao1105.2010)
783 [2010.](https://doi.org/10.3137/Ao1105.2010)

784
785 Hannula, H. R., Lemmetyinen, J., Kontu, A., Derksen, C., and Pulliainen, J.: Spatial and temporal variation of bulk snow
786 properties in northern boreal and tundra environments based on extensive field measurements, *Geosci Instrum Meth*, 5, 347-
787 363, [doi:10.5194/gi-5-347-2016](https://doi.org/10.5194/gi-5-347-2016), 2016.

788
789 Hartten, L. M. and Khalsa, S. J. S.: The H-K Variable SchemaTable developed for the YOPPsiteMIP (1.2), Zenodo,
790 <https://doi.org/10.5281/zenodo.6463464>, 2022.

791
792 Hinkel, K.M. and Nelson, F.E.: Anthropogenic heat island at Barrow, Alaska, during winter: 2001-2005, *J Geophys*
793 *Research*, 112, <https://doi.org/10.1029/2006JD007837>, 2007.

794
795 Holt, J.: Merged Observatory Data File (MODF) for Ny Alesund, Norwegian Meteorological Institute, [dataset](https://doi.org/10.21343/Y89M-6393),
796 <https://doi.org/10.21343/Y89M-6393>, 2023.
797
798 Huang, L., Mariani, Z., & Crawford, R.: MODF for Erik Nielsen Airport, Whitehorse, Canada during YOPP SOP1 and
799 SOP2, Norwegian Meteorological Institute, [dataset](https://doi.org/10.21343/A33E-J150), <https://doi.org/10.21343/A33E-J150>, 2023a.
800
801 Huang, L., Mariani, Z., & Crawford, R.: MODF for Iqaluit Airport, Iqaluit, Nunavut, Canada during YOPP SOP1 and
802 SOP2, Norwegian Meteorological Institute, [dataset](https://doi.org/10.21343/YRNF-CK57), <https://doi.org/10.21343/YRNF-CK57>, 2023b.
803
804 Illingworth, A. J., Cimini, D., Gaffard, C., Haeffelin, M., Lehmann, V., Lohnert, U., O'Connor, E. J., and Ruffieux, D.:
805 Exploiting Existing Ground-Based Remote Sensing Networks to Improve High-Resolution Weather Forecasts, *B Am*
806 *Meteorol Soc*, 96, 2107-2125, [doi: 10.1175/Bams-D-13-00283.1](https://doi.org/10.1175/Bams-D-13-00283.1), 2015.
807
808 Joe, P., Melo, S., Burrows, W. R., Casati, B., Crawford, R. W., Deghan, A., Gascon, G., Mariani, Z., Milbrandt, J., and
809 Strawbridge, K.: The Canadian Arctic Weather Science Project Introduction to the Iqaluit Site, *B Am Meteorol Soc*, 101,
810 E109-E128, [doi: 10.1175/Bams-D-18-0291.1](https://doi.org/10.1175/Bams-D-18-0291.1), 2020.
811
812 Jung, T., Gordon, N. D., Bauer, P., Bromwich, D. H., Chevallier, M., Day, J. J., Dawson, J., Doblas-Reyes, F., Fairall, C.,
813 Goessling, H. F., Holland, M., Inoue, J., Iversen, T., Klebe, S., Lemke, P., Losch, M., Makshtas, A., Mills, B., Nurmi, P.,
814 Perovich, D., Reid, P., Renfrew, I. A., Smith, G., Svensson, G., Tolstykh, M., and Yang, Q. H.: Advancing Polar Prediction
815 Capabilities on Daily to Seasonal Time Scales, *B Am Meteorol Soc*, 97, 1631-+, [doi: 10.1175/Bams-D-14-00246.1](https://doi.org/10.1175/Bams-D-14-00246.1), 2016.
816
817 Kochendorfer, J., M. Earle, D. Hodyss, A. Reverdin, Y-A. Roulet, R. Nitu, R. Rasmussen, S. Landolt, S. Buisan, and T.
818 Laine: Undercatch Adjustments for Tipping-Bucket Gauge Measurements of Solid Precipitation. *J. Hydrometeor.*, 21, 1193-
819 1205, <https://doi.org/10.1175/JHM-D-19-0256.1>, 2020.
820
821 Koltzow, M., Casati, B., Bazile, E., Haiden, T., and Valkonen, T.: An NWP Model Intercomparison of Surface Weather
822 Parameters in the European Arctic during the Year of Polar Prediction Special Observing Period Northern Hemisphere 1,
823 *Weather Forecast*, 34, 959-983, [doi: 10.1175/Waf-D-19-0003.1](https://doi.org/10.1175/Waf-D-19-0003.1), 2019.
824
825 Lawrence, H., Bormann, N., Sandu, I., Day, J., Farnan, J., and Bauer, P.: Use and impact of Arctic observations in the
826 ECMWF Numerical Weather Prediction system, *Q J Roy Meteor Soc*, 145, 3432-3454, [doi: 10.1002/qj.3628](https://doi.org/10.1002/qj.3628), 2019.
827
828 Lesins, G., Duck, T. J., and Drummond, J. R.: Climate trends at Eureka in the Canadian high arctic, *Atmos Ocean*, 48, 59-80,
829 [doi: 10.3137/AO1103.2010](https://doi.org/10.3137/AO1103.2010), 2010.
830
831 Long, C. N. and Shi, Y.: An Automated Quality Assessment and Control Algorithm for Surface Radiation Measurements,
832 *Open Atmospheric Science Journal*, 23-37, [doi: 10.2174/1874282300802010023](https://doi.org/10.2174/1874282300802010023), 2008.
833
834 Luojus, K., Pulliainen, J., Takala, M., Lemmetyinen, J., Mortimer, C., Derksen, C., Mudryk, L., Moisan, M., Hiltunen,
835 M., Smolander, T., Ikonen, J., Cohen, J., Salminen, M., Norberg, J., Veijola, K., and Venalainen, P.: GlobSnow v3.0

Formatted: Font color: Blue

Formatted: Font color: Blue

Formatted: Font color: Blue

Formatted: Font color: Blue

836 Northern Hemisphere snow water equivalent dataset, *Sci Data*, 8, ARTN 463, <https://doi.org/10.1038/s41597-021-00939-2>,
837 2021.

838

839 Mariani, Z., Crawford, R., Casati, B., and Lemay, F.: A Multi-Year Evaluation of Doppler Lidar Wind-Profile Observations
840 in the Arctic, *Remote Sens-Basel*, 12, ARTN 323, [10.3390/rs12020323](https://doi.org/10.3390/rs12020323), <https://doi.org/10.3390/rs12020323>, 2020.

841

842 Mariani, Z.; Hicks-Jalali, S.; Strawbridge, K.; Gwozdecky, J.; Crawford, R.W.; Casati, B.; Lemay, F.; Lehtinen, R.;
843 Tuominen, P. (2021). Evaluation of Arctic Water Vapor Profile Observations from a Differential Absorption Lidar. *Remote*
844 *Sens.* 2021, 13, 551. <https://doi.org/10.3390/rs13040551>, 2021.

845

846 Mariani, Z., Dehghan, A., Gascon, G., Joe, P., Hudak, D., Strawbridge, K., and Corriveau, J.: Multi-Instrument Observations
847 of Prolonged Stratified Wind Layers at Iqaluit, Nunavut, *Geophys Res Lett*, 45, 1654-1660, doi: 10.1002/2017gl076907,
848 2018.

849

850 Mariani, Z., Hicks-Jalali, S., Strawbridge, K., Gwozdecky, J., Crawford, R. W., Casati, B., Lemay, F., Lehtinen, R., and
851 Tuominen, P.: Evaluation of Arctic Water Vapor Profile Observations from a Differential Absorption Lidar, *Remote Sens-*
852 *Basel*, 13, ARTN 551, [10.3390/rs13040551](https://doi.org/10.3390/rs13040551), 13(4), 551, <https://doi.org/10.3390/rs13040551>, 2021.

853

854 Mariani, Z., Huang, G., Crawford, R., Blanchet, J. P., Hicks-Jalali, S., Mekis, E., Pelletier, P., Rodriguez, P., and
855 Strawbridge, K.: Enhanced automated meteorological observations at the Canadian Arctic weather science (CAWS)
856 supersites, *Earth System Science Data*, 2022-14, 4995-5017, <https://doi.org/10.5194/essd-14-4995-2022>, 2022.

857

858 Maturilli, M., Herber, A., and König-Langlo, G.: *Climatology and time series of surface meteorology in Ny-Ålesund, Svalbard,*
859 *Earth Syst. Sci. Data*, 5, 155-163, <https://doi.org/10.5194/essd-5-155-2013>, 2013.

860

861 Maturilli, M.: Basic and other measurements of radiation at station Ny-Ålesund (2006-05 et seq). Alfred Wegener Institute -
862 Research Unit Potsdam, PANGAEA, <https://doi.org/10.1594/PANGAEA.914927>, 2020a.

863

864 Maturilli, M.: Continuous meteorological observations at station Ny-Ålesund (2011-08 et seq). Alfred Wegener Institute -
865 Research Unit Potsdam, PANGAEA, <https://doi.org/10.1594/PANGAEA.914979>, 2020b.

866

867 Maturilli, M.: High resolution radiosonde measurements from station Ny-Ålesund (2017-04 et seq). Alfred Wegener Institute
868 - Research Unit Potsdam, PANGAEA, <https://doi.org/10.1594/PANGAEA.914973>, 2020c.

869

870 Maturilli, M.: Ceilometer cloud base height from station Ny-Ålesund (2017-08 et seq). Alfred Wegener Institute - Research
871 Unit Potsdam, PANGAEA, <https://doi.org/10.1594/PANGAEA.942331>, 2022.

872

873 Maturilli, M., Hanssen-Bauer, I., Neuber, R., Rex, M., and Edvardsen, K.: The Atmosphere above Ny-Ålesund – Climate
874 and global warming, ozone and surface UV radiation / Hop, H. and Wiencke, C. (editors), *Advances in Polar Ecology, The*
875 *Ecosystem of Kongsfjorden, Svalbard*, Springer, ISBN: 978-3-319-46423-7, doi:10.1007/978-3-319-46425-1_2, 2019.

876

877 Mikola, J., Virtanen, T., Linkosalmi, M., Vaha, E., Nyman, J., Postanogova, O., Rasanen, A., Kotze, D. J., Laurila, T.,
878 Juutinen, S., Kondratyev, V., and Aurela, M.: Spatial variation and linkages of soil and vegetation in the Siberian Arctic

Formatted: c-bibliographic-information__value

879 tundra - coupling field observations with remote sensing data, Biogeosciences, 15, 2781-2801, [doi: 10.5194/bg-15-2781-](https://doi.org/10.5194/bg-15-2781-2018)
880 2018, 2018.

881

882 Morris, S. M. and Akish, E.: A-M Variable [&and](#) Attribute Template Table developed for the YOPPSiteMIP (1.2), Zenodo,
883 <https://doi.org/10.5281/zenodo.6974550>, 2022.

884

885 NCCS: Climate in Svalbard 2100 – a knowledge base for climate adaptation, [2018-ISSN 2387-3027](#),
886 <http://dx.doi.org/10.25607/OBP-888>, 2018.

887

888 O'Connor, E.: Merged observation data file for Sodankyla, Norwegian Meteorological Institute, [dataset](#),
889 <https://doi.org/10.21343/M16P-PQ17>, 2023.

890

891 Ohmura, A., Dutton, E.G., Forgan, B., Frohlich, C., Gilgen, H., Hegner, H., Heimo, A., Konig-Langlo, G., McArthur, B.,
892 Muller, G., Philipona, R., Pinker, R., Whitlock, C.H., Dehne, K., and Wild, M.: Baseline Surface Radiation Network
893 (BSRN/WCRP): New Precision Radiometry for Climate Research, B Am Meteorol Soc, 79, 2115-2136,
894 [https://doi.org/10.1175/1520-0477\(1998\)079<2115:BSRNBW>2.0.CO;2](https://doi.org/10.1175/1520-0477(1998)079<2115:BSRNBW>2.0.CO;2), 1998.

895

896 Persson, O. and Stone, R.: Evidence of forcing of Arctic regional climates by mesoscale processes, AMS Symposium on
897 Connection Between Mesoscale Processes and Climate Variability, San Antonio, Texas, 15-16 January 2007, 2.6,
898 https://ams.confex.com/ams/87ANNUAL/techprogram/paper_119015.htm, 2007.

899

900 ~~Pinard, J. D. J. P., Benoit, R., and Yu, W.: A WEST wind climate simulation of the mountainous Yukon, Atmos Ocean, 43,~~
901 ~~259-282, DOI 10.3137/ao.430306, 2005.~~

902

903 Pollard, W. H. and Bell, T.: Massive Ice Formation in the Eureka Sound Lowlands: A Landscape Model, PERMAFROST -
904 Seventh International Conference, Yellowknife, Canada, Collection Nordicana, 1998.

905

906 Pollard, W. H., Ward, M. A., and Becker, M. S.: The Eureka Sound lowlands: an ice-rich permafrost landscape in transition,
907 Dept. of Geography, McGill University, <https://members.cgs.ca/documents/conference2015/GeoQuebec/papers/402.pdf>,
908 2015.

909

910 Prakash, G., Shrestha, B., Younkin, K., Jundt, R., Martin, M., and Elliott, J.: Data Always Getting Bigger—A Scalable DOI
911 Architecture for Big and Expanding Scientific Data, 1, 11, 2016.

912

913 Rantanen, M., Karpechko, A. Y., Lipponen, A., Nordling, K., Hyvarinen, O., Ruosteenoja, K., Vihma, T., and Laaksonen,
914 A.: The Arctic has warmed nearly four times faster than the globe since 1979, Commun Earth Environ, [3, ARTN 168](#)
915 <https://doi.org/10.1038/s43247-022-00498-3>, 2022.

916

917 Rautiainen, K., Parkkinen, T., Lemmetyinen, J., Schwank, M., Wiesmann, A., Ikonen, J., Derksen, C., Davydov, S.,
918 Davydova, A., Boike, J., Langer, M., Drusch, M., and Pulliainen, J.: SMOS prototype algorithm for detecting autumn soil
919 freezing, Remote Sens Environ, 180, 346-360, [doi: 10.1016/j.rse.2016.01.012](https://doi.org/10.1016/j.rse.2016.01.012), 2016.

920

Formatted: Font color: Blue

Formatted: Font color: Blue

921 Sellmann, P.V., Brown, J., Lewellen, R., McKim, H.L., Merry, C.J.: The classification and geomorphic implications of thaw
922 lakes on the Arctic coastal plain, Alaska. Cold Regions Research and Engineering Laboratory (CRREL); CRREL-No. 344,
923 <https://hdl.handle.net/11681/5852>, 1975.

924

925 Shupe, M.D.: Clouds at Arctic Atmospheric Observatories. Part II: Thermodynamic Phase Characteristics, *J Appl Meteorol*
926 *Clim*, 50, 645-661, <https://doi.org/10.1175/2010JAMC2468.1>, 2011.

927

928 Shupe, M.D., Walden, V.P., Eloranta, E., Uttal, T., Campbell, J.R., Starkweather, S.M., and Shiobara, M.: Clouds at Arctic
929 Atmospheric Observatories. Part I: Occurrence and Macrophysical Properties, *J Appl Meteorol Clim*, 50, 626-644,
930 <https://doi.org/10.1175/2010JAMC2467.1>, 2011.

931

932 Stone, R.S., Dutton, E.G., Harris, J.M., and Longenecker, D.: Earlier spring snowmelt in northern Alaska as an indicator of
933 climate change, *J Geophys Research*, 107, <https://doi.org/10.1029/2000JD000286>, 2002.

934

935 Tremblay, S., Picard, J.-C., Bachelder, J. O., Lutsch, E., Strong, K., Fogal, P., Leaitch, W. R., Sharma, S., Kolonjari, F., Cox,
936 C. J., Chang, R. Y.-W. and Hayes, P. L.: Characterization of aerosol growth events over Ellesmere Island during the
937 summers of 2015 and 2016, *Atmos. Chem. Phys.*, 19, 5589-5604, [doi: 10.5194/acp-19-5589-2019](https://doi.org/10.5194/acp-19-5589-2019).

938

939 Uttal, T., Makshtas, A. and Laurila, T.: The Tiksi International Hydrometeorological Observatory - An Arctic Members
940 Partnership, *WMO Bulletin Vol 62 (1) – 2013*, 2013.

941

942 Uttal, T., Hartten, L.M., Khalsa, S.J., Casati, B., Svensson, G., Day, J., Gallagher, M., Holt, J., Akish, E., Morris, S.,
943 O'Connor, E., Pirazzini, R., Huang, L., Crawford, R., Mariani, Z., Godoy, Ø., Tjernström, J.A.K., Prakesh, G., Hickmon, N.,
944 Maturilli, M., and Cox, C.: Merged Observatory Data Files (MODFs): An Integrated Research Data Product Supporting
945 Process Oriented Investigations and Diagnostics, *2023/2024, submitted to Model Intercomparison and Improvement Projects*
946 *(MIIPs) for the polar regions and beyond (GMD/ESSD inter-journal SI) submitted October 17, 2023 – under review 2024*.

947

948 Verlinde, J., Zak, B. D., Shupe, M. D., Ivey, M. D., and Stamnes, K.: The ARM North Slope of Alaska (NSA) Sites, *Meteor*
949 *Mon*, 57, [doi: 10.1175/Amsmonographs-D-15-0023.1](https://doi.org/10.1175/Amsmonographs-D-15-0023.1), 2016.

950

951 Weaver, D., Strong, K., Schneider, M., Rowe, P. M., Sioris, C., Walker, K. A., Mariani, Z., Uttal, T., McElroy, C. T.,
952 Vömel, H., Spassiani, A., and Drummond, J. R.: Intercomparison of atmospheric water vapour measurements at a
953 Canadian High Arctic site, *Atmos. Meas. Tech.*, 10, 2851–2880, <https://doi.org/10.5194/amt-10-2851-2017>, 2017.

954

955 Widener, K., Bharadwaj, N., and Johnson, K.: Ka-Band ARM Zenith Radar (KAZR) Instrument Handbook, United States
956 Department of Energy (USDOE), <https://doi.org/10.2172/1035855>, 2012.

957

958 WMO: Guide to Meteorological Instruments and Methods of Observation. WMO-No.8, Geneva, Switzerland, ISBN: 978-
959 92-63-10008-5, <https://library.wmo.int/idurl/4/68662>, 2021.

960

961 Wohner, C., Peterseil, J., and Klug, H.: Designing and implementing a data model for describing environmental monitoring
962 and research sites, *Ecol Inform*, 70, [ARTN 101708https://doi.org/10.1016/j.ecoinf.2022.101708, 2022](https://doi.org/10.1016/j.ecoinf.2022.101708),
963 [10.1016/j.ecoinf.2022.101708, 2022](https://doi.org/10.1016/j.ecoinf.2022.101708).

964
965 Younkin, K. and Long, C.: Improved Correction of IR Loss in Diffuse Shortwave Measurements: An ARM Value-Added
966 Product, PNNL; Richland, WA, United States, Medium: ED, [doi: 10.2172/1020732](https://doi.org/10.2172/1020732), 2003.
967

968
969
970

971
972

973 **Table 1.** List of facility coordinates for locations where $MODF_{vsm}$ measurements were collected at each site. The measured variables that
974 are observed at each site are listed (refer to Table 3). In some cases, the same variable is measured at multiple locations for a single site;
975 these observations and their corresponding coordinates are embedded within the MODF.

	Facility Name	Coordinates	Measured Variables
	Whitehorse	Whitehorse N60.71, W135.07	All
	Iqaluit	Iqaluit N63.74, W68.51	All
	Sodankylä	Operative Sounding Station Area; Automatic Weather Station (LUOxxxx) N67.366618 - N67.367220, E26.628253 - E26.63144	Pressure, Visibility
		CO2 Flux Mast Area (VUOxxxx) N67.361883, E26.643003 - E26.64323	Total precipitation of water, all wind, vertical velocity, temperature, dew-point temperature, relative humidity, snow thickness, all radiation, cloud base height
		Intensive Observation Area (IOAxxxx) N67.361654 - N67.361950, E26.633190 - E26.634191	Temperature, relative humidity, snow thickness, snowfall flux, snow water equivalent, all short-wave radiation, soil temperature profile, soil moisture, snow temperature
		Lichen Fence (JAKxxxx) N67.36710 - N67.36716, E26.634740 - E26.63513	All radiation
		Micrometeorological Mast Area (METxxxx) N67.361711 - N67.36216, E26.63726 - E26.65117	All wind, temperature, vertical velocity, relative humidity, snow thickness, all radiation, all heat fluxes, friction velocity, soil temperature profile, soil moisture, snow temperature
		Peatland Area (SUOxxxx) N67.361903 - N67.36707, E26.633802 - E26.654067	Temperature, dew-point temperature, relative humidity, snow thickness, all short-wave radiation, soil temperature profile, soil moisture, snow temperature
	Utqiagvik	ARM Facility N71.19228, W156.3654	All except ozone concentration, snow thickness, and soil temperature profile
		GML Barrow Atmospheric Baseline Observatory N71.3230, W156.6114	Ozone concentration, snow thickness, and soil temperature profile
	Tiksi	Baseline Surface Radiation Network (BSRN) N71.5862, E128.9188	All radiation observations
		Fluxtower N71.595, E128.882	All except radiation observations
	Ny- Ålesund	Baseline Surface Radiation Network (BSRN) N78.92278, E11.92725	All radiation observations, pressure, cloud base height
		AWIPEV Met.Tower N78.92226, E11.92667	All wind, temperature, relative humidity, specific humidity
		Balloon Launch Facility N78.92301, E11.92271	All timeSeriesProfileSonde observations
	Eureka	Baseline Surface Radiation Network (BSRN) N79.989, W85.9404	All radiation observations

"All" refers to the entire list of the measured variables in Table 3, whereas "All radiation" refers to all radiation-related measured variables.

Formatted: Font: Not Bold

Formatted Table

Formatted: Font: Not Bold

Formatted: Font: Not Bold

Formatted: Font: Not Bold

Formatted: Font: Not Bold

Formatted: Font: Not Bold

Formatted: Font: Not Bold

Fluxtower	N80.083, W86.417	Pressure, all wind, temperature, relative humidity, snow thickness, ground heat flux, soil temperature profile
Sonde Launch	N79.9833, W85.9333	All timeSeriesProfileSonde observations

Table 1. List of facility coordinates for locations where $MODF_{y_{sm}}$ measurements were collected at each of the supersite locations. The variables (listed in Table 3) that are measured at each location are listed.

980 **Table 2.** List of final DOIs for each site's MODF_{YMB}.

981 ~~In some cases, the same variable is measured at multiple locations for a single site; these observations and their corresponding coordinates~~
982 ~~are embedded within the MODF.~~

983

984

985

DOI	Title	Citation
Whitehorse , https://doi.org/10.21343/a33e-j150	MODF for Erik Nielsen Airport, Whitehorse, Canada during YOPP SOP1 and SOP2	Huang et al., 2023a
Iqaluit , https://doi.org/10.21343/yymf-ck57	MODF for Iqaluit Airport, Iqaluit, Nunavut, Canada during YOPP SOP1 and SOP2	Huang et al., 2023b
Sodankylä , https://doi.org/10.21343/m16p-pq17	Merged observation data file for Sodankylä	O'Connor, 2023
Utqiagvik , https://doi.org/10.21343/a2dx-nq55	MODF for Utqiagvik, Alaska, during YOPP SOP1 and SOP2	Akish & Morris, 2023c
Tiksi , https://doi.org/10.21343/5bwn-w881	MODF for Tiksi, Russia, during YOPP SOP1 and SOP2	Akish & Morris, 2023b
Ny-Ålesund , https://doi.org/10.21343/y89m-6393	Merged Observatory Data File (MODF) for Ny Ålesund	Holt, 2023
Eureka , https://doi.org/10.21343/r85j-tc61	MODF for Eureka, Canada, during YOPP SOP1 and SOP2	Akish & Morris, 2023a

Formatted: Font: Not Bold

Formatted: Font: Not Bold

Formatted: Font: Not Bold

Formatted Table

Formatted: Font: Not Bold

Formatted: Font: Not Bold

Formatted: Font: Not Bold

Formatted: Font: Not Bold

Formatted: Font: Not Bold

Formatted: Font: Not Bold

Formatted: Font: Not Bold

986

987

988

989 **Table 3.** List of the geophysical variables currently included in each site's MODF. Note that this table only includes variables
990 currently in the existing MODF_{ysm}, and does not indicate the complete list of variables that are observed at each site. **Table 2.**
991 List of final DOIs for each of the supersite's MODF_{ysm}.
992

Total precipitation of water in all phases per unit area ($\text{kg m}^{-2} \text{s}^{-1}$)	near-surface (2m, 10m)				
Eastward Wind (m s^{-1})	near-surface (2m, 10m)	near-surface (18m, 32m, 38m, 48m)	near-surface (2m, 10m, 20m, 40m)	near-surface (2m, 10m)	near-surface (6m, 11m)
Northward Wind (m s^{-1})	near-surface (2m, 10m)	near-surface (18m, 32m, 38m, 48m)	near-surface (2m, 10m, 20m, 40m)	near-surface (2m, 10m)	near-surface (6m, 11m)
Temperature (K)	near-surface (2m, 10m)	near-surface (3m, 8m, 18m, 32m, 48m)	near-surface (2m, 10m, 20m, 40m)	near-surface (2m, 6m, 10m)	near-surface (2m, 10m)
Dew-point Temperature (K)	near-surface (2m, 10m, 20m, 40m)				
Relative Humidity (1 or %)	near-surface (2m, 10m)	near-surface (3m, 8m, 18m, 32m, 48m)	near-surface (2m, 10m, 20m, 40m)	near-surface (2m, 6m, 10m)	near-surface (2m, 6m, 10m)
Soil Temperature Profile (K)	sub-surface (5cm, 30cm)		sub-surface (5cm, 10cm, 15cm, 20cm, 25cm, 30cm, 45cm, 70cm, 95cm, 120cm)	sub-surface (5cm, 10cm, 15cm, 20cm, 25cm, 30cm, 45cm, 70cm, 95cm, 120cm)	sub-surface (5cm, 10cm, 15cm, 20cm, 25cm, 30cm, 45cm, 70cm, 95cm, 120cm)
Soil Moisture (kg m^{-3})	sub-surface (5cm, 30cm)				
Snow Temperature (K)	near-surface (10cm, 20cm, 30cm, 40cm, 50cm, 60cm, 70cm, 80cm, 90cm, 100cm, 110cm)				
timeSeriesProfilesSonde Variables	Atmospheric pressure (Pa)	radiosonde	radiosonde	radiosonde	radiosonde
	Eastward Wind (m s^{-1})	radiosonde	radiosonde	radiosonde	radiosonde
	Northward Wind (m s^{-1})	radiosonde	radiosonde	radiosonde	radiosonde
	Temperature (K)	radiosonde	radiosonde	radiosonde	radiosonde
	Dew-point Temperature (K)	radiosonde	radiosonde	radiosonde	radiosonde
	Specific Humidity (1 or kg kg^{-1})				Radiosonde
	Relative Humidity (1 or %)	radiosonde	radiosonde	radiosonde	radiosonde

* Denotes a variable NOT included in the H-K Table
 ** Denotes a calculated variable (not a direct observation)

Table 3. List of the geophysical variables currently included in each supersite's MODF. Note that this table only includes variables currently in the existing MODF_{psm} and does not indicate the complete list of variables that are observed at each site. An asterisk (*) denotes a variable not included in the H-K table and a double asterisk (**) denotes a calculated variable.

Formatted: Superscript

Formatted: Superscript

Formatted: Superscript

Formatted: Superscript

Formatted: Superscript

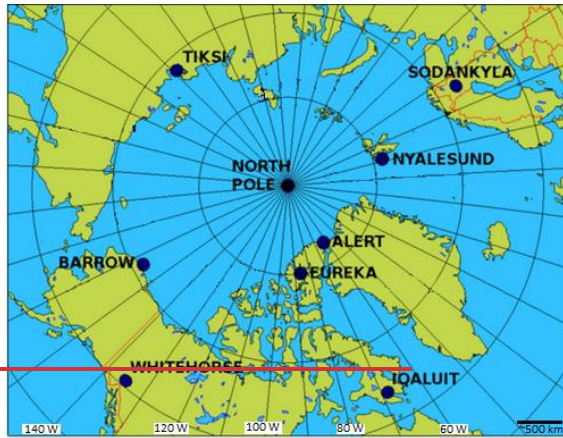
Formatted: Superscript

Formatted: Superscript

Formatted: Superscript

Formatted: Font: Not Bold

a)



b)



1007
1008
1009
1010

1011
1012

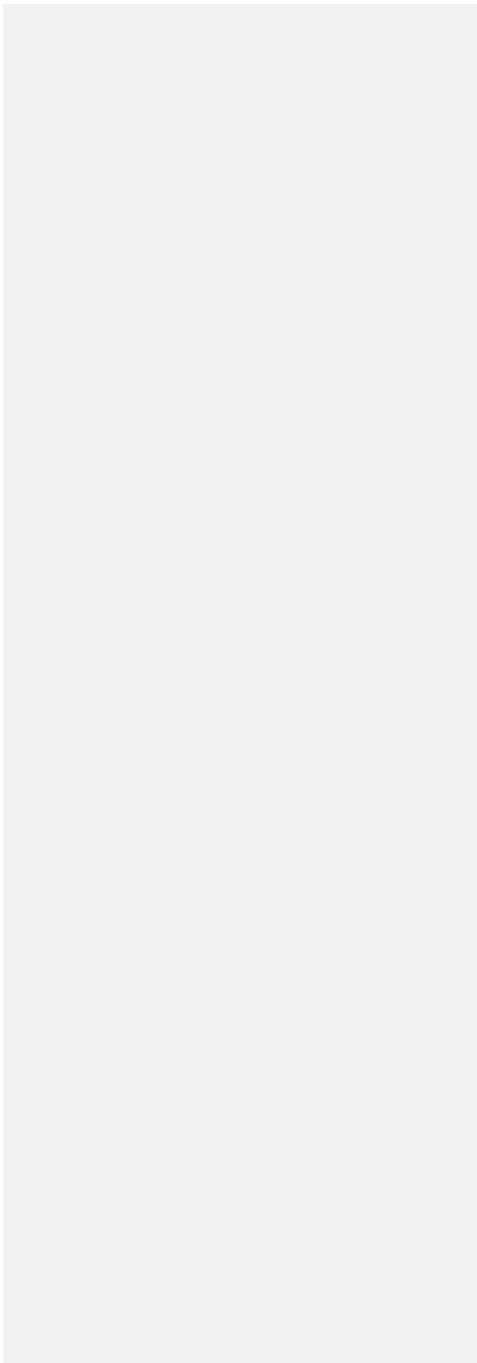


Table 4. List of the instruments that contributed to the Whitehorse MODF, including details about the instrument manufacturer, measured variables, configuration, temporal resolution, measurement uncertainty, and quality control applied. Unless otherwise stated in the instrument configuration column, all instruments were deployed at 2 m a.g.l. The MODF featureType timeSeries variables are listed first, with timeSeriesProfile and timeSeriesProfileSonde variables listed last. * Denotes a variable NOT included in the H-K Table.

<u>Measured variables</u>	<u>Instrument</u>	<u>Manufacturer</u>	<u>Instrument Configuration</u>	<u>Temporal Resolution</u>	<u>Uncertainty (+/-)</u>	<u>Quality Control</u>
<u>Atmospheric pressure (Pa)</u>	WXT520	Vaisala	Solid-state, all-in-one weather instrument in standard aspirated configuration mounted on a pole.	1 min	0.5 hPa	Observations that fell outside of the 3-sigma normal climatological range were rejected, as were observations that had a rate of change greater than a seasonal-dependant threshold (e.g., >20 hPa/hr change).
<u>Total precipitation of water in all phases per unit area (kg m⁻² s⁻¹)</u>			No bird spike kit was used.		5%	Observations that fell outside of the 3-sigma normal climatological range were rejected, as were observations that had a rate of change greater than a seasonal-dependant threshold (e.g., > 10 mm/hr change). No corrections for solid precipitation under-catchment were performed (the dataset is raw in the MODF); where appropriate, users are recommended to process under-catchment corrections via Kochendorfer et al. (2020).
<u>Eastward Wind (m s⁻¹)</u>					0.3 ms ⁻¹	Observations that fell outside of the 3-sigma normal climatological range were rejected, as were observations that had a rate of change greater than a seasonal-dependant threshold (e.g., > 10 m/s/hr change).
<u>Northward Wind (m s⁻¹)</u>						
<u>Temperature (K)</u>					0.3 K	The shelter heating effect is uncorrected. Observations that fell outside of the 3-sigma normal climatological range were rejected, as were observations that had a rate of change greater than a seasonal-dependant threshold (e.g., > 5 K/hr change).
<u>Relative Humidity (1 or %)</u>					3%	The humidity is not corrected in a sub-freezing environment. Observations that fell outside of the 3-sigma normal climatological range were rejected, as were observations that had a rate of change greater than a seasonal-dependant threshold (e.g., > 30 %/hr change).
<u>Dew-point Temperature (K)</u>					0.5 K	The shelter heating effect is uncorrected and humidity is not corrected in a sub-freezing environment. Observations that fell outside of the 3-sigma normal climatological range were rejected, as were observations that had a rate of change

						greater than a seasonal-dependant threshold (e.g., > 5 K/hr change).
<u>Cloud Base Height (m)</u>	<u>CL51</u>	<u>Vaisala</u>	<u>Proprietary algorithm determines the lowest cloud base height</u>	<u>1 min</u>	<u>~10 m</u>	<u>No additional QC performed.</u>
<u>Atmospheric pressure (Pa)</u>	<u>RS92 / DFM-09</u>	<u>Vaisala / GRAW</u>	<u>Standard radiosonde launch</u>	<u>6 hr</u>	<u>0.5 hPa</u>	<u>Data were binned into 10-meter intervals of geopotential height and all measurements within each bin were averaged.</u>
<u>Eastward Wind (m s⁻¹)</u>					<u>0.15 ms⁻¹</u>	<u>No additional QC performed.</u>
<u>Northward Wind (m s⁻¹)</u>						
<u>Temperature (K)</u>					<u>0.15 K</u>	
<u>Dew-point Temperature (K)</u>					<u>0.5 K</u>	

1018
1019

Table 5. Same as Table 4, except for the Iqaluit MODF.

<u>Measured variables</u>	<u>Instrument</u>	<u>Manufacturer</u>	<u>Instrument Configuration</u>	<u>Temporal Resolution</u>	<u>Uncertainty (+/-)</u>	<u>Quality Control</u>
<u>Pressure (Pa)</u>	PTB110	Vaisala	Installed within a naturally vented protective enclosure.	1 min	0.3 hPa	Observations that fell outside of the 3-sigma normal climatological range were rejected, as were observations that had a rate of change greater than a seasonal-dependant threshold (e.g., >20 hPa/hr change).
<u>Total precipitation of water in all phases per unit area (kg m⁻² s⁻¹)</u>	Pluvio2	OTT	Single Alter shield		5%	Observations that fell outside of the 3-sigma normal climatological range were rejected, as were observations that had a rate of change greater than a seasonal-dependant threshold (e.g., > 10 mm/hr change). No corrections for solid precipitation under-catchment were performed (the dataset is raw in the MODF); where appropriate, users are recommended to process under-catchment corrections via Kochendorfer et al. (2020).
<u>Eastward Wind (m s⁻¹)</u>	Wind monitor 5103	RM Young	Four-blade helicoid propeller in standard configuration with a wind vane to measure wind direction		0.3 ms ⁻¹	Observations that fell outside of the 3-sigma normal climatological range were rejected, as were observations that had a rate of change greater than a seasonal-dependant threshold (e.g., > 10 m/s/hr change).
<u>Northward Wind (m s⁻¹)</u>						
<u>Temperature (K)</u>	HMP35D	Vaisala	Sensor installed in shaded, naturally vented shelter.		0.1 K	The shelter heating effect is uncorrected. Observations that fell outside of the 3-sigma normal climatological range were rejected, as were observations that had a rate of change greater than a seasonal-dependant threshold (e.g., > 5 K/hr change).
<u>Dew-point Temperature (K)</u>					0.2 K	The shelter heating effect is uncorrected and humidity is not corrected in a sub-freezing environment. Observations that fell outside of the 3-sigma normal climatological range were rejected, as were observations that had a rate of change greater than a seasonal-dependant threshold (e.g., > 5 K/hr change).
<u>Relative Humidity (1 or %)</u>					0.8%	The humidity is not corrected in a sub-freezing environment. Observations that fell outside of the 3-sigma normal climatological range were rejected, as were observations that had a rate of change greater than a seasonal-dependant threshold (e.g., > 30 %/hr change).
<u>Snow thickness (m)</u>	SR50A	Campbell Scientific	Sonic distance sensor at 50KHz with a perforated flat target		1 cm	Observations that fell outside of the 3-sigma normal climatological range were rejected, as were observations that had a rate of change

			base levelled at the surface (0 m a.g.l.)		greater than a seasonal-dependant threshold (e.g., > 20 cm/hr change).
<u>Upward Short-wave Radiation</u> (W m ⁻²)	<u>CMP10L</u> (285 to 2800 nm)	<u>Kipp and Zonen</u>	<u>Integrated levelling included, dome, RM Young radiation shield (6 plate), and a CVF4L Ventilation System with Integrated Heater running when</u>	<u>7 W m⁻²</u>	<u>Data is raw and no additional QC was performed.</u>
<u>Downward Short-wave Radiation</u> (W m ⁻²)			<u>temperatures where near zero to prevent frost.</u>		<u>No additional QC was performed on these observations to account for potential frost or snow deposition on the sensors. Data should be treated with caution since they typically require additional QC processing prior to analysis.</u>
<u>Upward Long-wave Radiation</u> (W m ⁻²)	<u>CGR4L</u> (4.5 to 42 μm)	<u>Kipp and Zonen</u>	<u>Installed on the flux tower crossbeam arms.</u>	<u>7 W m⁻²</u>	
<u>Downward Long-wave Radiation</u> (W m ⁻²)					
<u>*Horizontal East-facing Long-wave Radiation</u> (W m ⁻²)					
<u>*Horizontal West-facing Long-wave Radiation</u> (W m ⁻²)					
<u>*Horizontal South-facing Long-wave Radiation</u> (W m ⁻²)					
<u>*Horizontal North-facing Long-wave Radiation</u> (W m ⁻²)					
<u>Cloud Base Height</u> (m)	<u>CL51</u>	<u>Vaisala</u>	<u>Proprietary algorithm determines the lowest cloud base height</u>	<u>5 m</u>	<u>No additional QC was performed.</u>
<u>Atmospheric pressure</u> (Pa)	<u>WXT520</u>	<u>Vaisala</u>	<u>Solid-state, all-in-one weather instrument in standard aspirated configuration mounted on a pole at 10 m a.g.l.</u>	<u>0.5 hPa</u>	<u>Observations that fell outside of the 3-sigma normal climatological range were rejected, as were observations that had a rate of change greater than a seasonal-dependant threshold (e.g., >20 hPa/hr change).</u>
<u>Total precipitation of water in all phases per unit area</u> (kg m ⁻² s ⁻¹)			<u>No bird spike kit used.</u>	<u>5%</u>	<u>Observations that fell outside of the 3-sigma normal climatological range were rejected, as were observations that had a rate of change greater than a seasonal-dependant threshold (e.g., > 10 mm/hr change).</u> <u>No corrections for solid precipitation under-catchment were performed (the dataset is raw in the MODF); where appropriate, users are</u>

recommended to process under-catchment corrections via Kochendorfer et al. (2020).

<u>Eastward Wind (m s⁻¹)</u>					<u>0.3 ms⁻¹</u>	Observations that fell outside of the 3-sigma normal climatological range were rejected, as were observations that had a rate of change greater than a seasonal-dependant threshold (e.g., > 10 m/s/hr change).
<u>Northward Wind (m s⁻¹)</u>						
<u>Temperature (K)</u>					<u>0.3 K</u>	Observations that fell outside of the 3-sigma normal climatological range were rejected, as were observations that had a rate of change greater than a seasonal-dependant threshold (e.g., > 5 K/hr change).
<u>Relative Humidity (1 or %)</u>					<u>3%</u>	The humidity is not corrected in a sub-freezing environment. Observations that fell outside of the 3-sigma normal climatological range were rejected, as were observations that had a rate of change greater than a seasonal-dependant threshold (e.g., > 30 %/hr change).
<u>Atmospheric pressure (Pa)</u>	<u>RS92 / DFM-09</u>	<u>Vaisala / GRAW</u>	<u>Standard radiosonde launch</u>	<u>6 hr</u>	<u>0.5 hPa</u>	Data were binned into 10-meter intervals of geopotential height and all measurements within each bin were averaged.
<u>Eastward Wind (m s⁻¹)</u>					<u>0.15 ms⁻¹</u>	No additional QC performed.
<u>Northward Wind (m s⁻¹)</u>						
<u>Temperature (K)</u>					<u>0.15 K</u>	
<u>Dew-point Temperature (K)</u>					<u>0.5 K</u>	

1021

1022

1023

Table 6. Same as Table 4, except for the Sodankylä MODF.

<u>Measured variables</u>	<u>Instrument</u>	<u>Manufacturer</u>	<u>Instrument Configuration</u>	<u>Temporal Resolution</u>	<u>Uncertainty (+/-)</u>	<u>Quality Control</u>
Temperature (K)	PT100	Vaisala	Sensor installed in shaded, naturally vented shelter.	10 min	0.1 K	The shelter heating effect is uncorrected. Observations that fell outside of the 3-sigma normal climatological range were rejected, as were observations that had a rate of change greater than a seasonal-dependant threshold (e.g., > 5 K/hr change).
	PT100	Generic			0.3 K	
	PT100	Pentronic			0.3 K	
	HMP155	Vaisala			0.1 K	
Relative Humidity (1 or %)	HMP155	Vaisala	Sensor installed in shaded, naturally vented shelter.		1%	The humidity is not corrected in a sub-freezing environment. Observations that fell outside of the 3-sigma normal climatological range were rejected, as were observations that had a rate of change greater than a seasonal-dependant threshold (e.g., > 30 %/hr change).
	HMP35D	Vaisala			0.8%	
	HMP45D	Vaisala			2% (0-90 %RH) 3% (90-100 %RH)	
Snow thickness (m)	SR50	Campbell Scientific	Sonic distance sensor at 50KHz with a perforated flat target base levelled at the surface (0 m a.g.l.)		1 cm	Observations were checked against site-based climatology ranges, routine manual observations, and the rate of change thresholds, which were based on hourly criteria. Observations that fell outside of the 3-sigma normal climatological range were rejected, as were observations that had a rate of change greater than a seasonal-dependant threshold (e.g., > 20 cm/hr change).
Total precipitation of water in all phases per unit area (kg m⁻² s⁻¹)	Distrometer Model: 5.4110.01.200	Thies Clima	Model with extended heating	1 min	5%	Observations that fell outside of the 3-sigma normal climatological range were rejected, as were observations that had a rate of change greater than a seasonal-dependant threshold (e.g., > 10 mm/hr change).
Snowfall flux unit area (kg m⁻² s⁻¹)						
Snow water equivalent (m)	SSG 1000	Sommer Messtechnik	Sensor consists of seven perforated panels having a total measuring surface of 2.8 x 2.4 m with the measurement being made on the centre plate.		0.3%	Data is raw and no additional QC was performed.
Downward Short-wave Radiation (W m⁻²)	CMA11 (285 to 2800 nm)	Kipp and Zonen	Integrated levelling included, dome, RM Young radiation shield (6 plate), and a CVF4L Ventilation System with Integrated Heater running	10 min	7 W m ⁻²	Data is raw and no additional QC was performed. No additional QC was performed on these observations to account for
				1 min	7 W m ⁻²	

<u>Surface horizontal visibility (m)</u>	FD12P	Vaisala	Optical forward-scatter sensor installed on a pole at 10 m a.g.l.	10%	Data is raw and no additional QC was performed.
<u>Eastward Wind (m s⁻¹)</u>	WA25 (WAA25 and WAV25)	Vaisala	Cup anemometer and vane designed for Arctic conditions with integrated heaters to prevent ice buildup. Deployed at 10 m a.g.l.	0.3 m s ⁻¹	Observations that fell outside of the 3-sigma normal climatological range were rejected, as were observations that had a rate of change greater than a seasonal-dependant threshold (e.g., > 10 m/s/hr change).
<u>Northward Wind (m s⁻¹)</u>					
<u>Eastward Wind (m s⁻¹)</u>	UA2D	Thies Clima	2-D sonic anemometer deployed at 10 m a.g.l.	2%	Data is raw and no additional QC was performed.
<u>Northward Wind (m s⁻¹)</u>					
<u>Eastward Wind (m s⁻¹)</u>	USA-1	Metek	3-D sonic anemometer deployed at 10 m a.g.l.	0.1 m s ⁻¹	Data is raw and no additional QC was performed.
<u>Northward Wind (m s⁻¹)</u>					
<u>Vertical velocity (m s⁻¹)</u>					
<u>Surface friction velocity (eddy covariance method) (m s⁻¹)</u>				0.1 m s ⁻¹	No additional QC performed. Additional filtering of output from eddy covariance processing not performed.
<u>Surface turbulent latent heat flux (eddy covariance method) (W m⁻²)</u>				20%	
<u>Surface turbulent sensible heat flux (eddy covariance method) (W m⁻²)</u>				20%	
<u>Surface momentum flux (eddy covariance method) (W m⁻²)</u>				25%	
<u>Ground heat flux (W m⁻²)</u>	HFP01	Hukseflux	Thermopile buried in soil	3%	Data is raw and no additional QC was performed.
<u>Bulk soil temperature (K)</u>	QMT103	Vaisala	Thin steel sheath incorporating sensor, buried in soil	0.3 K	
	Hydra Probe II	Stevens	4-needle sensor buried in soil	0.3 K	
<u>Average layer soil moisture (kg m⁻²)</u>	Hydra Probe II	Stevens	4-needle sensor buried in soil	5%	
<u>Bulk soil temperature (K)</u>	GS3	Decagon Devices	Sensor encapsulated in an epoxy body with stainless	1 K	

			<u>steel needles. Buried in soil.</u>			
<u>GTE</u>	<u>Decagon Devices</u>		<u>Sensor encapsulated in an epoxy body with stainless steel needles. Buried in soil.</u>		<u>1 K</u>	
<u>109-L</u>	<u>Campbell Scientific</u>		<u>Thermistor encapsulated in an epoxy-filled aluminum housing and buried in soil.</u>		<u>0.3 K</u>	
<u>CS655</u>	<u>Campbell Scientific</u>		<u>Two 12-cm-long stainless steel rods connected to a printed circuit board encapsulated in epoxy attached to a shielded cable. Buried in soil.</u>		<u>0.3 K</u>	
<u>PT100</u>	<u>Pentronic</u>		<u>Thin steel sheath incorporating sensor, buried in soil.</u>		<u>0.3 K</u>	
<u>IKES PT100</u>	<u>Nokeval</u>		<u>Thin steel sheath incorporates a Pt100 sensor with double insulation moulded in solid rubber with the cable. Buried in soil.</u>		<u>0.3 K</u>	
<u>Average layer soil moisture (kg m⁻²)</u>	<u>ThetaProbe ML2x</u>	<u>Delta-T Devices</u>	<u>4-needle sensor buried in soil</u>		<u>5.00%</u>	<u>Data is raw and no additional QC was performed</u>
<u>Snow temperature (K)</u>	<u>107-L</u>	<u>Campbell Scientific</u>	<u>Thermistor encapsulated in an epoxy-filled aluminum housing and buried in snow</u>		<u>0.5 K</u>	
<u>Air temperature (K)</u>	<u>PT100</u>	<u>generic</u>	<u>Sensor installed in shaded, naturally vented shelter. Deployed at 40 m a.g.l.</u>		<u>0.3 K</u>	
<u>Relative Humidity (1 or %)</u>	<u>HMP</u>	<u>Vaisala</u>	<u>Sensor installed in shaded, naturally vented shelter. Deployed at 40 m a.g.l.</u>		<u>0.80%</u>	
<u>Wind speed (m s⁻¹)</u>	<u>WAA25</u>	<u>Vaisala</u>	<u>Cup anemometer with integrated heater to prevent ice buildup. Deployed at 40 m a.g.l.</u>		<u>0.17 m s⁻¹</u>	
<u>Atmospheric pressure (Pa)</u>	<u>RS41</u>	<u>Vaisala</u>	<u>Standard radiosonde launch</u>	<u>6 hr</u>	<u>0.5 hPa</u>	<u>No additional QC was performed. Output is directly from Vaisala processing.</u>
<u>Eastward Wind (m s⁻¹)</u>					<u>0.15 ms⁻¹</u>	

Northward Wind
(m s⁻¹)

Temperature (K)

0.3 K

Relative Humidity
(1 or %)

4%

1025

1026

1027 **Table 7.** Same as Table 4, except for the Utqiagvik MODF.

<u>Measured variables</u>	<u>Instrument</u>	<u>Manufacturer</u>	<u>Instrument Configuration</u>	<u>Temporal Resolution</u>	<u>Uncertainty (+/-)</u>	<u>Quality Control</u>
<u>Pressure (Pa)</u>	PTB-220	Vaisala	The Barrow meteorology station (BMET) obtains barometric pressure, visibility, and precipitation data from sensors at the base of the tower. https://www.arm.gov/capabilities/instruments/twr	1 min	0.15 hPa	Observations were checked against other instrumentation on the tower and compared with the surface meteorological instruments and the energy balance Bowen ratio to remove outliers and nonphysical values.
<u>Near-surface (2m) eastward wind (m s⁻¹)</u>	WS425	Vaisala	Sensors are aspirated.		0.135 ms ⁻¹	Data was also compared with the SONDE data that was launched from the tower; https://www.arm.gov/publications/tech-reports/handbooks/twr_handbook.pdf
<u>Near-surface (2m) northward wind (m s⁻¹)</u>			The Barrow meteorology station (BMET) uses mainly conventional in situ sensors; these are mounted at 2 m a.g.l. See: https://www.arm.gov/capabilities/instruments/twr			
<u>Near-surface (2m) air temperature (K)</u>	HMT337 (previously HMP35D/HMP45D)	Vaisala			0.2 K	
<u>Near-surface (2m) dew point temperature (K)</u>					0.2 K	
<u>Near-surface (2m) relative humidity (%)</u>					1.7 %	
<u>Ozone concentration in air (mole fraction)</u>	TE149i	Thermo Scientific	Inlet line samples air from roof of station through filter, while instrument is housed inside station building. This data set contains continuous UV photometric data of surface level ozone collected at 6m above ground level.		1 ppb	Manual inspection of the data to ensure nonphysical values are filtered. See: https://www.ncej.noaa.gov/access/metadata/landing-page/bin/iso?id=gov.noaa.ncdc:C00894
<u>Surface snow thickness (m)</u>	Toughsonic 30	Senix	Instrument is located on broadband radiation albedo rack		n/a	Data is compared against meteorological and global radiation data to verify accuracy; data values not physically possible are removed. Pollution/technical events are flagged and/or removed from data set.
<u>Surface (skin) temperature (K)</u>	IRT	Apogee	Data collected from US Climate Reference Network (CRN) per standard operating configuration (see https://www1.ncdc.noaa.gov/pub/data/uscrn/documentation/progra		0.5 K	Inter-comparison of the 3 temperature sensors: Sensors should be within 0.3° C of one another. An hourly flag message is generated for any departure

			m/ManualMonitoringHandbook.pdf		greater than 0.30° C (i.e., 0.301° C and greater).
					<u>IR max should exceed the ambient temperature, and IR min should be less than ambient temperature, otherwise data is filtered. See : https://www1.ncdc.noaa.gov/pub/data/uscsm/documentation/program/ManualMonitoringHandbook.pdf</u>
Upward surface short-wave radiation (W m⁻²)	GNDRAD (0.3 to 3 μm)	PSP	Standard operating configuration, see: https://www.arm.gov/capabilities/instruments/gndrad	<u>2.0 W m⁻²</u>	SIRS Instrument mentors review the Data Quality Office's (DOO) weekly Data Quality Assessment Reports (DQAR). If a problem is detected, a Data Quality Problem Report (DQPR) is issued. The DQPR system is a web-based system by which the mentor, local site operations staff, and the DOO are informed and communicate to resolve a data quality problem (e.g., instrument failure, data collection issue, etc.). A DQPR is typically initiated by the DOO or instrument mentor during data review. This process filters and removes erroneous data.
Downward short-wave radiation at the surface (W m⁻²)	SKYRAD (295 to 3000 nm)	PSP	Standard operating configuration, see: https://www.arm.gov/capabilities/instruments/skyrad	<u>4.0 W m⁻²</u>	
Upward surface long-wave radiation (W m⁻²)	GNDRAD (4 to 50 μm)	PIR	Standard operating configuration, see: https://www.arm.gov/capabilities/instruments/gndrad	<u>2.0 W m⁻²</u>	
Downward surface long-wave radiation (W m⁻²)	SKYRAD (3.5 to 50 μm)	PIR	Standard operating configuration, see: https://www.arm.gov/capabilities/instruments/skyrad	<u>4.0 W m⁻²</u>	Data Quality Reports (DQR) are prepared by instrument mentors as needed to close out corresponding DQPRs. See: https://www.arm.gov/capabilities/instruments/gndrad and https://www.arm.gov/capabilities/instruments/skyrad
Surface turbulent latent heat flux (eddy covariance method) (W m⁻²)	Windmaster Pro Anemometer	Gill	Standard ARM site arrangement is sonic sensor "North" mark pointing along the boom to the tower; the boom is usually pointing due south; u wind component is north-south with positive toward the north; v wind component is east-west with positive toward the west.	<u><1.5%</u>	The QCECOR VAP currently contains two variables: surface latent heat flux (LH) and sensible heat flux (SH), together with their QC flags. When SEBS are collocated with ECOR, the wetness measurements from SEBS are used to flag the LH that may be incorrect due to hydrometeors such as precipitation, dew, or frost. An indeterminate flag is given to those that fail the wetness test. See: https://www.arm.gov/publications/tech_reports/doe-sc-arm-tr-223.pdf
Surface turbulent sensible heat flux (eddy covariance method) (W m⁻²)			No correction is made to convert u and v component into meteorological "north" and "east" wind components when tower boom is not aligned to south; u wind component is "along boom", v wind component is "cross boom" https://www.arm.gov/publications/tech_reports/doe-sc-arm-tr-223.pdf		

Ground heat flux ($W m^{-2}$)	HFT-3, SMP1, STP-1	Radiation and Energy Balance Systems, Inc.	Soil measurements are performed by three sets of soil heat flow (5 cm depth), soil temperature (0–5 cm average), and soil moisture (centered at 2.5 cm) probes. Soil heat flow is adjusted for the effect of soil moisture above the soil heat flow plate. The storage of energy in the soil above the soil heat flow plate is determined from the change in soil temperature with time.	10 mV	Instrument mentor routinely views graphic displays that include plots (day courses) of all calculated quantities and comparison plots (time series or scatter plots) of relevant parameters with data from collocated ECOR, SEBS, EBBR (SGP CF and EF39 only), and surface meteorological instrumentation (MET) (Cook et al. 2006). See: https://www.arm.gov/publications/tech_reports/handbooks/sebs_handbook.pdf
Eastward wind component ($m s^{-1}$)	WS425	Vaisala	Sensors are aspirated. The Barrow meteorology station (BMET) uses mainly conventional in situ sensors mounted at four different heights (2m, 10m, 20m and 40m) on a 40 m tower to obtain profiles of wind speed, wind direction, air temperature, dew point and humidity. https://www.arm.gov/capabilities/instruments/twr	0.135 ms^{-1}	Observations were checked against other instrumentation on the tower and compared with the surface meteorological instruments and the energy balance bowen ratio to remove outliers and nonphysical values. Data was also compared with the SONDE data that was launched from the tower: https://www.arm.gov/publications/tech_reports/handbooks/twr_handbook.pdf
Northward wind component ($m s^{-1}$)					
Air temperature (K)	HMT337 (previously HMP35D/HMP45D)	Vaisala		0.2 K	
Dew-point temperature (K)				0.2 K	
Relative humidity (%)				1.7 %	
Soil temperature profile (K)	PT100	in-house	Soil measurements are performed by three sets of soil heat flow (5 cm depth), soil temperature (0–5 cm average), and soil moisture (centered at 2.5 cm) probes. Soil heat flow is adjusted for the effect of soil moisture above the soil heat flow plate. The storage of energy in the soil above the soil heat flow plate is determined from the change in soil temperature with time.	n/a	Data is compared against meteorological and global radiation data to verify accuracy; pollution/technical events are flagged and/or removed from data set; data values not physically possible are removed
Snowfall flux per unit area	KAZR	KAZR	Installed on top of the ARM facility roof. See: https://doi.org/10.1525/elementa.2021.00101	n/a	Threshold-based flags to remove outliers and unphysical values. See: https://doi.org/10.1525/elementa.2021.00101 and: https://www.arm.gov/publications/tech_reports/handbooks/kazr_handbook.pdf
Atmospheric pressure (Pa)	RS41	Vaisala	Standard radiosonde launch.	6-12 hr 1 hPa	The manufacturer defines the cumulative sensor uncertainty at the 2-sigma (95.5%) confidence level.

<u>Eastward wind component (m s⁻¹)</u>	<u>The SONDE system originally located at Barrow was an old CLASS-type that was originally operated by NOAA's Climate Measurements and Diagnostics Laboratory on TWP's Manus site.</u>	<u>0.15 ms⁻¹</u>	<u>Repeatability is estimated from the standard deviation of differences between two successive repeated calibrations (2-sigma).</u>
<u>Northward wind component (m s⁻¹)</u>			<u>Reproducibility is estimated from the standard deviation of differences in twin soundings. See: http://dx.doi.org/10.5439/1595321.</u>
<u>Temperature (K)</u>		<u>0.5 K</u>	
<u>Dew-point temperature (K)</u>		<u>0.5 K</u>	
<u>Relative humidity (%)</u>		<u>5%</u>	

1028
1029
1030

Table 8. Same as Table 4, except for the Tiksi MODE.

<u>Measured variables</u>	<u>Instrument</u>	<u>Manufacturer</u>	<u>Instrument Configuration</u>	<u>Temporal Resolution</u>	<u>Uncertainty (+/-)</u>	<u>Quality Control</u>
<u>Surface pressure (Pa)</u>	PTB110	Vaisala	Located on the fluxtower at 5m a.g.l.	1 min	0.3 hPa	Data are manually QC'd to identify and eliminate instrument malfunction; outliers are filtered out if values are physically impossible.
<u>Near-surface (4m) eastward wind (m s⁻¹)</u>	3001	RM Young	Located on the fluxtower at 4m a.g.l.		0.5 m s ⁻¹	
<u>Near-surface (4m) northward wind (m s⁻¹)</u>						
<u>Near-surface air temperature (K)</u>	HMT330	Vaisala	Located on the fluxtower		0.2 K	
<u>Near-surface relative humidity (%)</u>					1.5 + 0.015 × reading	
<u>Surface snow thickness (m)</u>	SR50A	Campbell Scientific	Located on the albedo rack		1 cm	
<u>Surface (skin) temperature (K)</u>	SI-111	Apogee	Located on the fluxtower		0.2 K	
<u>Upward surface short-wave radiation (W m⁻²)</u>	PSP (295-2800 nm)	Eppley	Located on the albedo rack		2.0 W m ⁻²	
<u>Downward surface short-wave radiation (W m⁻²)</u>	CM22 (200 to 3600 nm)	Kipp & Zonen	Located on the tracker at the MET station building		5.0 W m ⁻²	
<u>Upward surface long-wave radiation (W m⁻²)</u>	PIR (4 to 50 μm)	Eppley	Located on the albedo rack		2.0 W m ⁻²	
<u>Downward surface long-wave radiation (W m⁻²)</u>			Located on the tracker at the MET station building		4.0 W m ⁻²	
<u>Ground heat flux (W m⁻²)</u>	HPF01	Hukseflux	Located at the base of the fluxtower at 5cm depth		3 %	
<u>Air temperature (K)</u>	HMT330, HMP155	Vaisala	Located on the fluxtower at 2m, 6m, 10m a.g.l.		0.2 K	
<u>Relative humidity (%)</u>					1.5 + 0.015 × reading	
<u>Soil temperature profile (K)</u>	TP-101	MRC	Located at albedo rack at depths: 5cm, 10cm, 15cm, 20cm, 25cm, 30cm, 45cm, 70cm, 95cm, 120cm		n/a	
<u>Atmospheric pressure (Pa)</u>	RS41	Vaisala	Standard radiosonde launch.	12 hr	1 hPa	No additional QC was performed. See: https://www.ncei.noaa.gov/pub/data/igra/data/data-por/
<u>Eastward wind component (m s⁻¹)</u>			See: https://www.ncei.noaa.gov/pub/data/igra/data/data-por/		0.15 ms ⁻¹	
<u>Northward wind component (m s⁻¹)</u>						

Temperature (K)

0.5 K

Dew-point temperature (K)

0.5 K

Relative humidity (%)

5%

1032

1033

1034

Table 9. Same as Table 4, except for the Ny-Ålesund MODF.

<u>Measured variables</u>	<u>Instrument</u>	<u>Manufacturer</u>	<u>Instrument Configuration</u>	<u>Temporal Resolution</u>	<u>Uncertainty (+/-)</u>	<u>Quality Control</u>
Pressure (Pa)	DigiQuarz 6000-16B	Paroscientific, Inc.	Installed within a naturally vented protective enclosure.	1 min	0.08 hPa	Observations were checked against site-based climatology ranges and the rate of change thresholds. Flagged data was filtered.
Total precipitation of water in all phases per unit area ($\text{kg m}^{-2} \text{s}^{-1}$)	Pluvio2	OTT	Single Alter shield. Operated and analysed by the University of Cologne.		5%	No additional QC was applied; data is raw and should be treated with caution.
Eastward Wind (m s^{-1})	Combined Wind Transmitter 4.3324.32.073	Thies Clima	Opto-electronically scanned three-cup anemometer with low starting speed. The position of the wind vane is detected opto-electronically.		0.4 ms^{-1}	Instrument is checked on a daily basis manually by the instrument mentor. Observations were checked against site-based climatology ranges, the rate of change thresholds, and redundant measurements in close proximity if/when possible. Erroneous or unphysical observations were filtered.
Northward Wind (m s^{-1})						
Temperature (K)	Ventilated air temperature transmitter 2.1265.20.000	Thies Clima	The sensor is protected by a double thermal radiation shield. A built-in ventilator provides for the necessary air flow.		0.1 K	
Relative Humidity (1 or %)	HMP155	Vaisala	The sensor with additional temperature sensor is installed in a vented radiation shelter.		0.80%	
Upward Short-wave Radiation (W m^{-2})	CMP22 (200 to 3600 nm)	Kipp and Zonen	Sensor installed in an Eigenbrodt ventilation system to prevent from icing.		5 Wm^{-2}	Instrument is checked on a daily basis manually by the instrument mentor. Data quality check is performed according to BSRN requirements.
Downward Short-wave Radiation (W m^{-2})			Sensor installed in an Eigenbrodt ventilation system to prevent from icing.			
Upward Long-wave Radiation (W m^{-2})	PIR (4 to 50 μm)	Eppley	Sensor installed in an Eigenbrodt ventilation system to prevent from icing.		5 Wm^{-2}	
Downward Long-wave Radiation (W m^{-2})			Sensor is shaded and installed in an Eigenbrodt ventilation system to prevent from icing.			
Cloud Base Height (m)	CL51	Vaisala	Proprietary algorithm determines the lowest cloud base height		~10 m	Operated with the standard Vaisala proprietary algorithm that retrieves cloud base height. Additional check for unphysical outliers was manually performed by the instrument mentor.

<u>Atmospheric pressure (Pa)</u>	<u>RS41</u>	<u>Vaisala</u>	<u>Standard radiosonde launch</u>	<u>6 hr</u>	<u>0.5 hPa</u>	<u>No additional QC was performed.</u>
<u>Eastward Wind (m s⁻¹)</u>					<u>0.15 ms⁻¹</u>	
<u>Northward Wind (m s⁻¹)</u>						
<u>Temperature (K)</u>					<u>0.3 K</u>	
<u>Relative Humidity (1 or %)</u>					<u>4%</u>	

1036
1037
1038
1039

Table 10. Same as Table 4, except for the Eureka MODF.

<u>Measured variables</u>	<u>Instrument</u>	<u>Manufacturer</u>	<u>Instrument Configuration</u>	<u>Temporal Resolution</u>	<u>Uncertainty (+/-)</u>	<u>Quality Control</u>
<u>Surface pressure (Pa)</u>	PTB220	Vaisala	Located on Flux Tower at 2 m a.g.l.	1 min	0.3 hPa	Data are manually QC'd to identify and eliminate instrument malfunctions by the instrument mentor. Outliers are filtered out if values are physically impossible.
<u>Near-surface (6m) eastward wind (m s⁻¹)</u>	VENTUS-UMB Ultrasonic	Lufft	Located on Flux Tower at 6 m	1-10 s	0.1 ms ⁻¹	
<u>Near-surface (6m) northward wind (m s⁻¹)</u>						Values are compared to other local variables if/when possible by the instrument mentor.
<u>Near-surface (2m) air temperature (K)</u>	HMT-337	Vaisala	Located on Flux Tower	1 min	0.2 K	
<u>Near-surface (2m) relative humidity (%)</u>					1.5 + 0.015 × reading	
<u>Surface Snow Thickness</u>	SR50A	Campbell Scientific	Located on Flux Tower		1 cm	
<u>Surface (skin) temperature (K)</u>	IRTS-P	Apogee	Located on Flux Tower		0.2 K	
<u>Upward surface short-wave radiation (W m⁻²)</u>	PSP (295-2800 nm)	Eppley	Located on Flux Tower at 11 m a.g.l.		2.0 W m ⁻²	Processed through Long QCRad; Historical Quality Control Techniques: Long, C. N., & Shi, Y. (2008). See: doi: 10.2174/1874282300802010023
<u>Downward surface short-wave radiation (W m⁻²)</u>	CMP22 (200 to 3600 nm)	Kipp and Zonen			5.0 W m ⁻²	
<u>Upward surface long-wave radiation (W m⁻²)</u> ¹⁾	PIR (4 to 50 μm)	Eppley			4.0 W m ⁻²	
<u>Downward surface long-wave radiation (W m⁻²)</u>						
<u>Ground heat flux (W m⁻²)</u>	HPFO1	Hukseflux	Depth 3 cm		3 %	Manually QC'd to identify and eliminate instrument malfunctions or non physical values by the instrument mentor.
<u>Air temperature (K)</u>	HMT-337	Vaisala	Located on Flux Tower at 2, 6, 10 m.		0.2 K	Data are manually QC'd to identify and eliminate instrument malfunctions by the instrument mentor. Outliers are filtered out if values are physically impossible.
<u>Relative humidity (%)</u>					1.5 + 0.015 × reading	
<u>Soil temperature profile (K)</u>	TP-101	MRC	Depth: 5cm, 10cm, 15cm, 20cm, 25cm, 30cm, 45cm, 70cm, 95cm, 120cm		n/a	

<u>Eastward wind component (m s⁻¹)</u>	<u>VENTUS-UMB Ultrasonic</u>	<u>Lufft</u>	<u>Located on Flux Tower at 6 m and 11 m</u>	<u>1-10 s</u>	<u>0.1 ms⁻¹</u>	<u>Values are compared to other local variables if/when possible, by the instrument mentor.</u>
<u>Northward wind component (m s⁻¹)</u>						
<u>Atmospheric pressure (Pa)</u>	<u>RS41</u>	<u>Vaisala</u>	<u>Standard radiosonde launch</u>	<u>6 hr</u>	<u>0.5 hPa</u>	<u>No additional QC was performed.</u>
<u>Eastward Wind (m s⁻¹)</u>					<u>0.15 ms⁻¹</u>	
<u>Northward Wind (m s⁻¹)</u>						
<u>Temperature (K)</u>					<u>0.3 K</u>	
<u>Relative Humidity (1 or %)</u>					<u>4%</u>	

1041
1042
1043
1044
1045

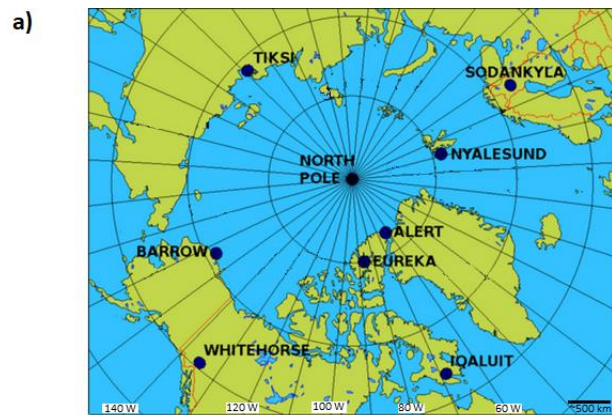


Figure 1. a) Locations of the MODF_{ysm} YOPP supersites (Antarctic supersites not shown). (b) Infographic depicting iconic building(s) at each supersite. The infographic is roughly centred around the North Pole (centre). All locations shown have generated a MODF_{ysm}, with the exception of Alert (in progress).

Formatted: Font color: Auto

Formatted: Font: 9 pt

Formatted: Space After: 10 pt, Line spacing: single, Bottom: (No border), Top: (No border), Bottom: (No border), Left: (No border), Right: (No border), Between : (No border)

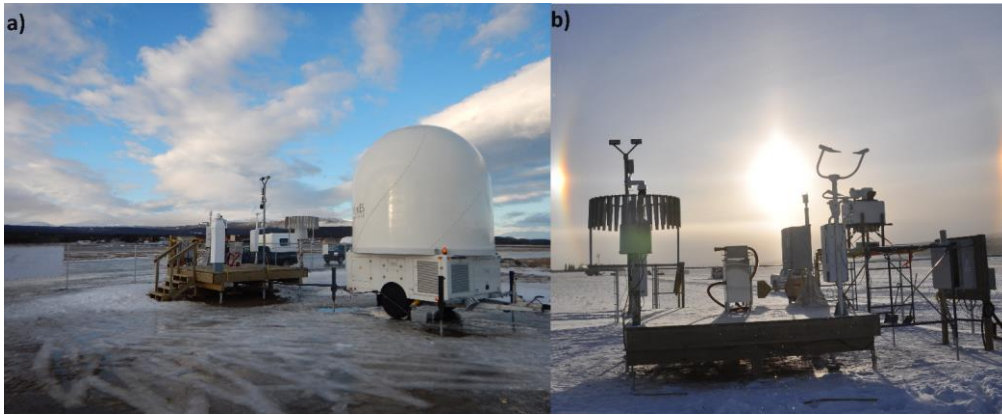


Figure 2. The Whitehorse site and the surrounding airfield in early spring 2018 with an X-band radar (white dome) in the foreground (a), and the main instrument platform, including a Pluvio2, Parsivel, FS11P, WXT520, and CL51 ceilometer (from left to right) with a sundog in the background (b). Photos adapted from Figure 5 in Mariani et al. (2022).

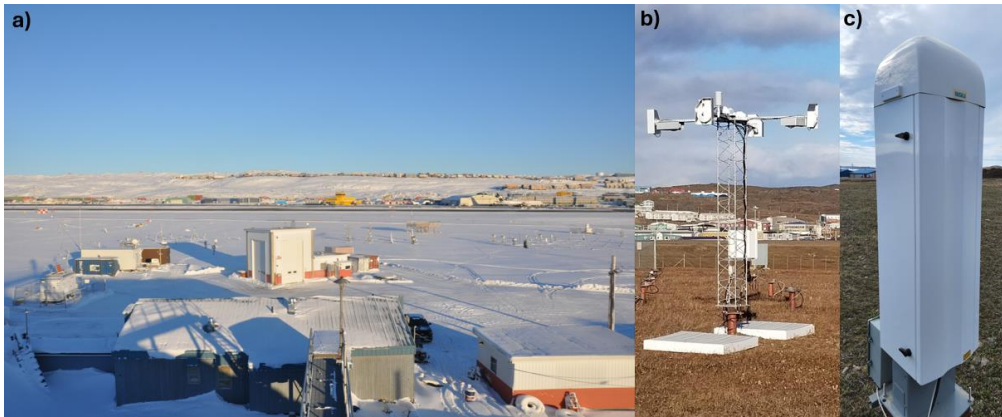
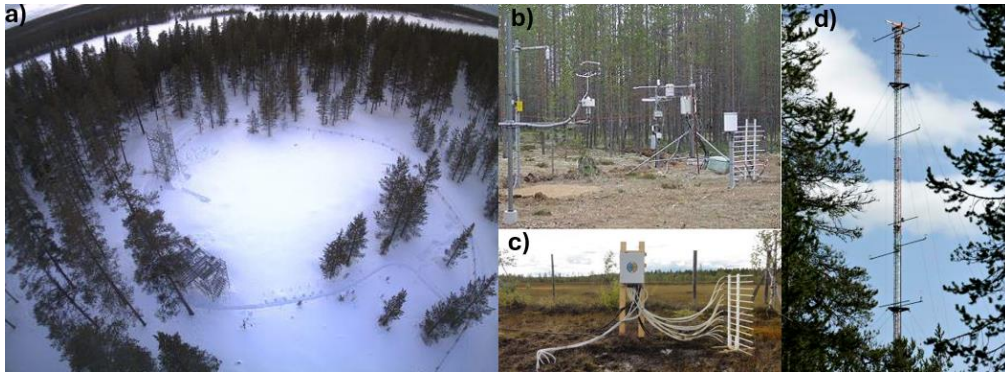
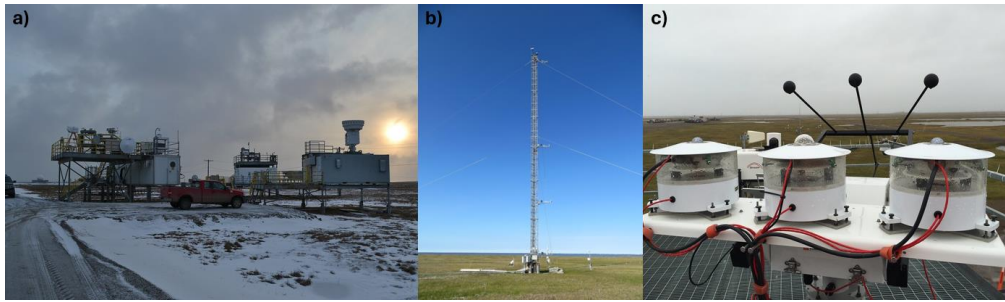


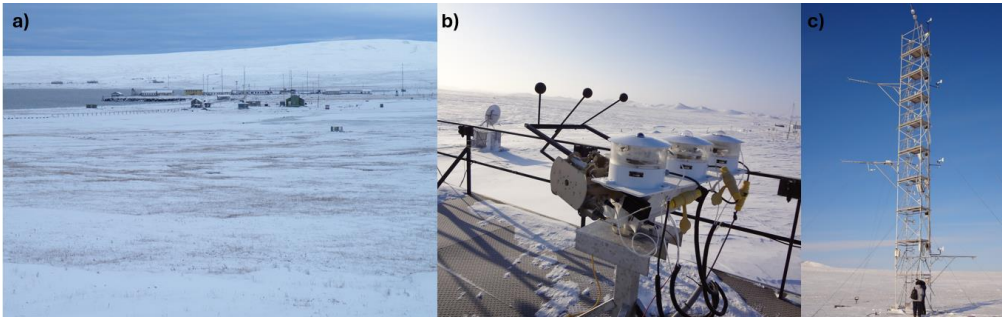
Figure 3. The Iqaluit site surroundings taken in winter 2018 with the Iqaluit airport in the background (a), the radiation flux sensor suite during the summer, consisting of several CMP10Ls, CGR4Ls, and SR50As (b), and the CL51 ceilometer during the summer (c). Photos adapted from Figure 2 (Mariani et al., 2022).



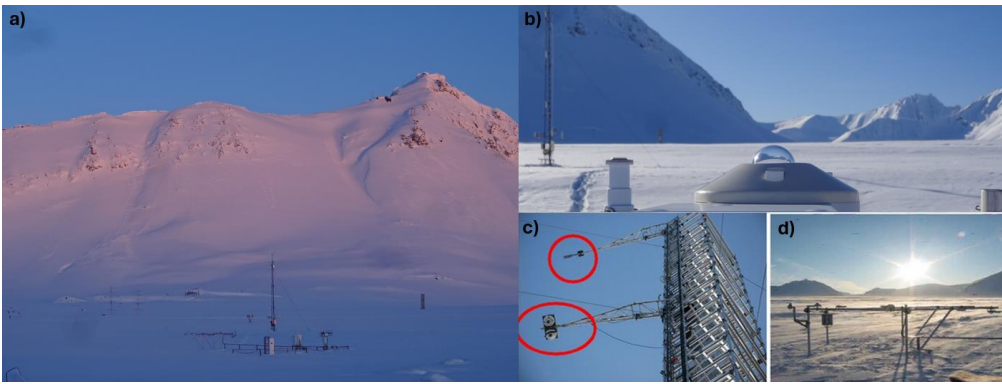
1062
1063 **Figure 4.** The Sodankylä site surroundings during the winter at the Intensive Observation Area, IOA, in the boreal forest (a), snow, soil and
1064 meteorological measurements in the MET measurement field (b), multi-level snow and soil measurements at the Peatland site, SUO, (c) and
1065 the meteorological tower with meteorological and radiation sensors (d). Photos: FMI (litdb.fmi.fi).
1066



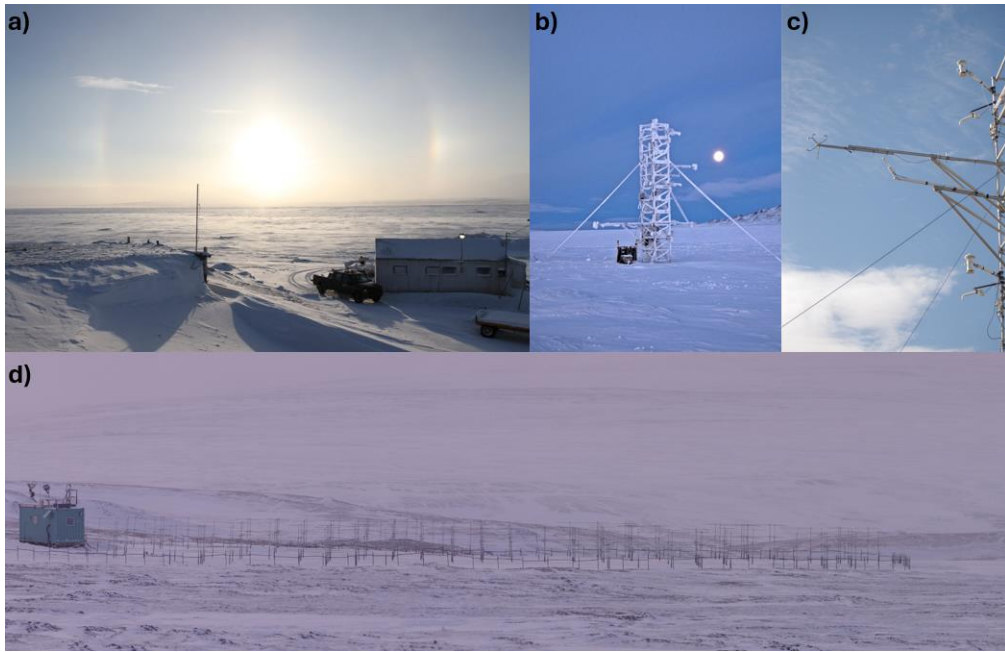
1068
1069 **Figure 5.** The Utqiaġvik site surroundings during the winter, including the main observation stations and their rooftop instrument suites (a),
1070 the meteorological tower with radiation flux sensors deployed in the summer (b), and the SKYRAD downward longwave radiation sensor
1071 deployed on the roof in the spring (c). Photos: www.arm.gov.
1072



1073
1074 **Figure 6.** The Tiksi site surroundings, taken from afar in the winter (a), the SKYRAD downward longwave radiation sensor deployed on
1075 the roof of the Tiksi observation building (b), and the meteorological tower equipped with radiation flux sensors (c). Photos: Taneil Uttal
1076 (NOAA).



1077
1078
1079 **Figure 7.** The Ny-Ålesund site surroundings taken in the winter with the meteorological sensors and radiation tower in the foreground (a),
1080 the CMP22 downward shortwave radiation sensor at the site (b), the meteorological tower with the radiation flux sensors circled (c), and
1081 several surface meteorological and albedo-measuring sensors at the BSRN station (d). Photos (c-d) are adapted from Figure 1 in Becherini
1082 et al., 2021.



1084
1085 **Figure 8.** The Eureka site surroundings in the winter, facing south from the Eureka Weather Station (EWS) looking over the frozen fjord
1086 with a sundog in the background (a), the meteorological tower at the Surface and Atmospheric Flux Irradiance Extension (SAFIRE)
1087 (b) with radiation flux (e.g., PSP) and meteorological sensors deployed (c), and the SAFIRE site surroundings taken from afar (d).

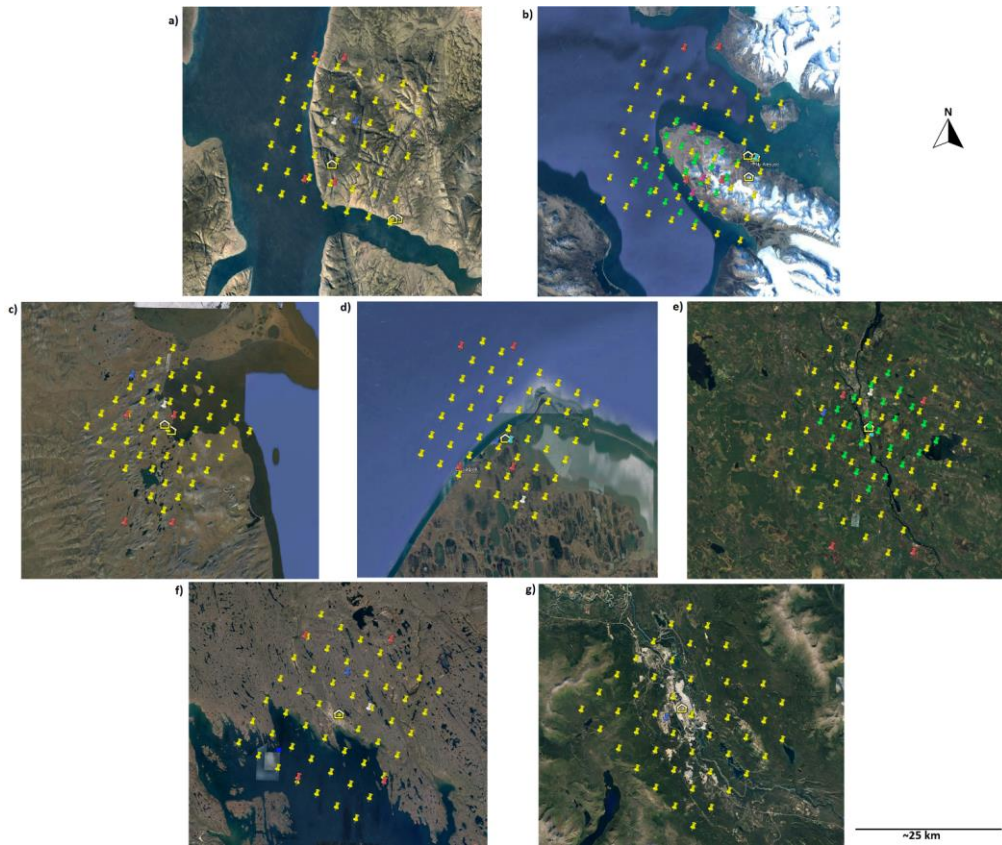


Figure 29. Model grid points at and around each [supersitesite](#) (a) Eureka, (b) Ny-Ålesund, (c) Tiksi, (d) Utqiagvik, (e) Sodankylä, (f) Iqaluit, and (g) Whitehorse, displayed through the Google Earth web-platform: *Image Landsat / Copernicus, Image ©2023 Maxar Technologies*. Sites are organized from highest latitude (Eureka) to lowest (Whitehorse). Yellow building icons represent the location of the facility on-site which contains all co-located instruments. Similarly, icons for the AROME-Arctic model grid are indicated by a green pin, ARPEGE pins are in white, DWD-ICON pins are light blue, ECCC-CAPS pins are yellow, ECMWF-IFS pins are dark blue, and SL-AV pins are in red. All images are north-aligned, nadir view.

1090

1091

1092

1093

1094

1095

1096

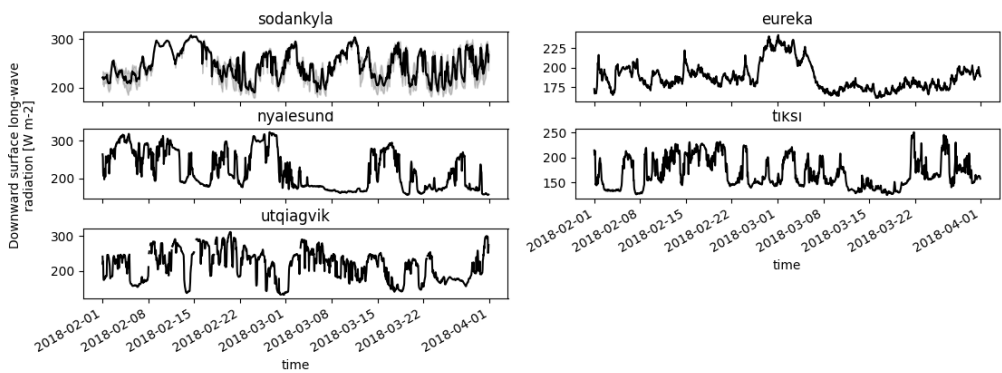
1097

1098

1099

1100

1101



1102

1103

1104

1105

1106

1107

Figure 310. Observations (30-min) of downward surface long-wave radiation (“rlds”) conducted during SOP1 at each supersitesite. Observations from Whitehorse and Iqaluit were not available during SOP1. Sodankylä conducts multiple observations of rlds; the mean (black line) and min/max spread in observed rlds (grey shaded area) are shown.

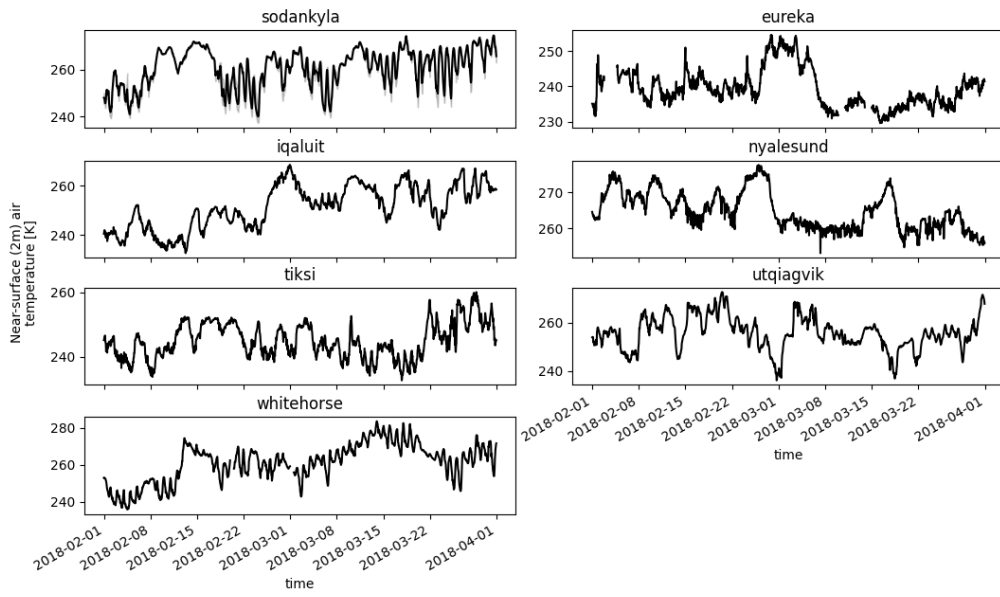
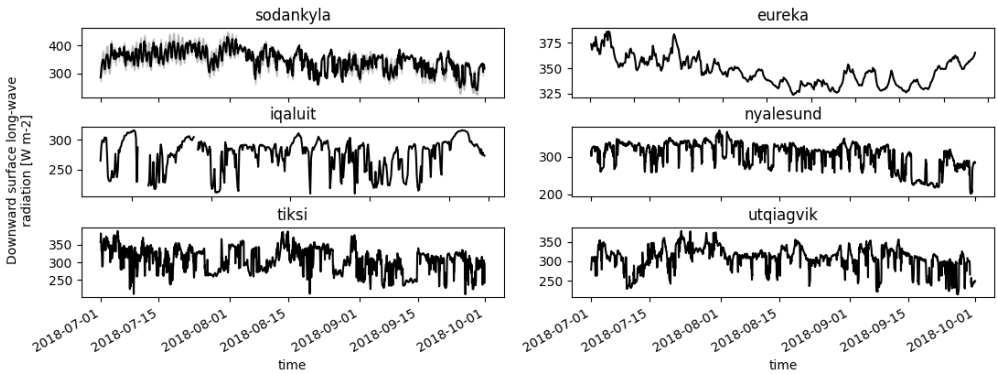


Figure 411. Similar to Figure 3, except for observations of near-surface (2 m) air temperature (“tas”) conducted at each [supersite](#) during SOP1.

1108
 1109
 1110
 1111

1112

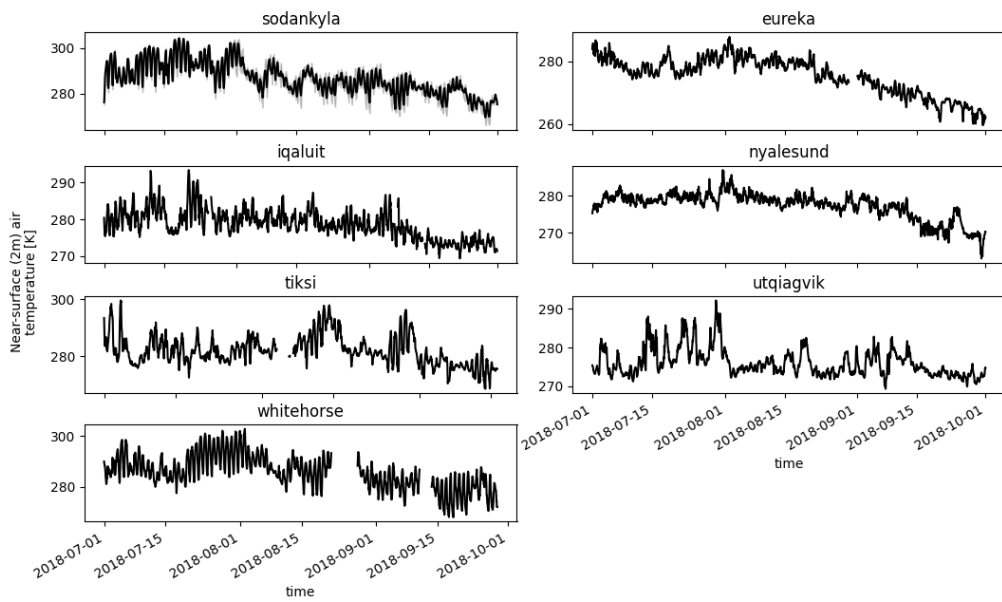


1113

1114 **Figure 512.** Similar to Figure 3, except for observations of downward surface long-wave radiation (“rlds”) conducted during SOP2 at each
1115 [super-site](#). Observations from Whitehorse were not available during SOP2.

1116

1117



1118

1119
1120

Figure 6.13. Similar to Figure 3, except for observations of near-surface (2 m) air temperature (“tas”) conducted at each [supersite](#) during SOP2.